ISTITUTO NAZIONALE DI FISICA NUCLEARE

Sezione di Trieste

INFN/AE-93/04

25 gennaio 1993

G. Calucci and D. Treleani

EIKONAL DIAGRAMS IN MULTIPARTON SEMI-HARD INTERACTIONS

Servizio Documentazione
dei Laboratori Nazionali di Frascati

EIKONAL DIAGRAMS IN MULTIPARTON SEMI-HARD INTERACTIONS*

G. Calucci and D. Treleani

Dipartimento di Fisica Teorica dell'Università di Trieste, Trieste, I 34014 Italy
INFN, Sezione di Trieste, Italy

ABSTRACT

We study the set of eikonal diagrams, derived from perturbative QCD, at the lowest order in the coupling constant and with vacuum quantum number exchange, in the three body interaction of a high energy projectile parton with two different target partons. The contribution to the semi-hard component of the inelastic cross section is worked out by evaluating the leading behavior of all the dominant cut diagrams. The different cut amplitudes are shown to be proportional to one another, with the same weights of the cutting rules which have been derived in the context of multi-pomeron exchange. As a consequence of the dominant configuration in the loop integrals, corresponding to the projectile parton on shell between successive interactions, the process is represented by the simplest probabilistic picture, where the three-body interaction is factorized as the product of two-body interaction probabilities.

PACS numbers: 11.20.Dj, 11.80.La, 12.35.Eq, 13.85.Hd.

* Work partially supported by the Italian Ministry of University and of Scientific and Technological Research.

I. Introduction

Multiple interactions in the case of two-body parton scattering, for $s \to \infty$, $t/s \to 0$, with s and t the usual Mandelstam variables, have been systematically investigated both for an Abelian theory of interaction[1] and in QCD[2]. In the Abelian theory, the set of multiple interactions, which are obtained from the s-channel unitarization, corresponds to the eikonal diagrams. At a given order in the coupling constant g, the eikonal diagrams differ to one another only by the ordering of the exchanged quanta and the eikonal approximation is implemented by taking the leading behavior of the sum of all the diagrams. While each single eikonal diagram with loop integrals is proportional to a power of $\ln s$, as a result of the loop integrations on the longitudinal variables, the sum of all the eikonal diagrams, at a given order in the coupling constant, does not contain any $\ln s$. The leading behavior of each single diagram is canceled by a destructive interference between different terms, in such a way that, after summing all the terms, at a given order in the coupling constant, only a subleading contribution, without any power of $\ln s$, is left.

In the non Abelian case, each diagram is characterized by a different color matrix, so that different diagrams cannot be added any more as isospin scalars. In order to study the non Abelian case, one needs to introduce, at each order in the coupling constant, a set of isospin factors which acts as a base for decomposing all isospin factors of the Feynman diagrams at the same order. To that purpose the box-isospin factors have been introduced[3]. Using the Jacobi identity for the structure constants and the commutation rules of the generators of the algebra, one can express each isospin factor, at a given order in g, as a sum of box-isospin factors up to the same order in g. Increasing the perturbative order, the decomposition increases rapidly in complexity. The case of the sixth order is extensively discussed in ref.4 and the graphical representation of the corresponding box-isospin factors is shown in fig.1. A calculation through the tenth perturbative order, for the vector-meson vector-meson elastic scattering amplitude, is presented in ref.3, while, in ref.5, the analysis is generalized (up to the eight perturbative order) to the three and four body parton interaction. The perturbative analysis shows a remarkable pattern of regularity: The decomposition of all isospin factors, in terms of box-isospin factors, allows one to express the space-time part multiplying each box-isospin factor as an expansion in powers of g^2 and $\ln s$. All the coefficients of the

expansion conspire to replace the t-channel gluons of the Feynman diagram, at the lowest order in g and with color factor equal to the box-isospin factor, with Reggeized gluons[4,6]; namely by modifying each of the gluon propagators by a factor $s^{\alpha(q)}$, where q is the momentum of the corresponding gluon.

Within the Reggeized gluon scheme, which arises from the perturbative analysis, the relevant quantities to be considered are the sets of Feynman diagrams contributing to the same box-isospin diagram. One may distinguish two different kinds of box-isospin diagrams:

a- The ones without interactions among the exchanged lines, like graphs 1, 2 and 4 in fig.1, and

b- the ones with interactions among the exchanged lines, like graph 3 in fig.1.

In case a, the lowest order term in g of the space-time factor is given by the sum of all the space-time factors of the eikonal diagrams at the same order, namely it is the same as the contribution obtained by exchanging elementary vector mesons within an Abelian theory of interaction. One may also notice that, in case b, every lowest order term in g contains a power of $\ln s$ which grows with the number of horizontal lines.

A feature of gluon Reggeization, which we like to emphasize, is that, at a given order in g and for each box-isospin diagram, one needs to consider a whole set of Feynman diagrams, whose space-time parts have to be added coherently. The resulting behavior is very different from the behavior of each single diagram. The lowest order term of the space-time part of each box-isospin diagram of kind a is the precise analogous of the Abelian theory and, correspondingly, although each single diagram grows as a power of $\ln s$, the sum does not contain any more factors proportional to $\ln s$. While color factors can be reorganized in such a way that only a few of them multiply a space-time part with a leading behavior, a main point about Reggeization is that terms, leading at the lowest order, become subleading after keeping into account higher order corrections, so that only terms with the exchange of vacuum quantum numbers finally dominate. As a consequence, in the framework of Reggeized gluons, one does not learn about dominant terms in the amplitude by simply selecting Feynman diagrams with the criterion of the leading behavior at high energy. One should rather focus on the exchange of quantum numbers and sum the contributions obtained by projecting all the different Feynman diagrams which contribute to the given exchange of the quantum numbers. Moreover, because of interferences between different terms, it is not a consistent

procedure to take into account of the diagrams with a leading behavior only, while performing the sum.

On the other hand, the different attitude of selecting rather the QCD diagrams, with the leading behavior at large s, and limiting the analysis to the corresponding color factors, is often used to discuss higher order exchanges, in interactions involving many partons (LLA QCD[7]). The same criterion is used in ref.8 (section 3.3) to select the "inside" topology in order to discuss the different cuts of double ladder exchange diagrams, with the purpose to prove the validity of the A.G.K. cutting rules[9] in QCD.

Since the physical picture of the interaction is considerably different in the two approaches, we find useful to reconsider, within the optics of gluon reggeization, the relations among the different cuts of a definite QCD amplitude. We examine, therefore, a case which belongs to the category of the class of diagrams studied in references 3,4 and 5, allowing, nevertheless, a comparison with the analysis performed in ref.8. Most of the arguments, which have been produced in ref.8, are based, in fact, on considerations involving only the first step of the ladder. We are therefore allowed to analyze a simplest case, of three body parton interaction, where the exchanged ladders are replaced with box-diagrams. The least order in the coupling constant to be considered is eight, as a consequence. In fig.2 all Feynman diagrams, at the eight order in g, with the projectile exchanging two gluons with each of the two targets and with the exclusion of terms containing the three-or-four gluon vertex, are represented. In fig.2, and in fig.3 as well, the projectile is represented by the horizontal line in the middle of each graph, the target partons are the two horizontal lines in the top and the bottom and the four lines left are the exchanged gluons. The set of diagrams in fig.2 is the complete set of diagrams which contribute, at the lowest order in g, to the box-isospin diagram of kind a, with the quantum number exchange of two gluons in each of the t-channels. At the eight order in g, the base for the isospin factors is not unique[10]. Any of the color factors, of the 24 diagrams in fig.2, may be used to represent this base isospin diagram. Since the color factor, which is selected with the argument of the diagrams leading at high energy, corresponds to the "inside" topology, we choose, as isospin factor associated with the diagrams in fig.2, the diagram in fig.3.

We limit our analysis to the isospin term represented in fig.3, which is only one of the components in the much structured three body amplitude. The term, which we have selected is, however, simple enough to allow a rather detailed analysis. In

fact we keep into account of all the relevant subleading contributions both to the term in the amplitude, which we have selected, and also to all the corresponding different cuts of the amplitude. The role played by the subleading terms is, in this way, fully explicit. Our analysis shows that, because of destructive interferences between different diagrams, next to leading terms in $\ln s$ are of the same importance as the leading ones.

An interesting property of the sum of the space time parts of the diagrams of the set in fig.2 is that one of being gauge independent, at least in the case of the three quark interaction. The reason is that the set of diagrams in fig.2 is a complete set of diagrams, in electrodynamics, with a given quantum number exchange and at a given order in the coupling constant. The term under investigation, in the three-body parton amplitude, has, moreover, a close connection with the eikonal models of high energy hadronic and nuclear interactions[11]. In addition, as it will result by studying the cuts of the amplitude, it is directly related with the semi-hard rescattering of a high energy parton, which is expected to be a very frequent process in nuclear collisions at the energies of future Colliders[12].

The paper is organized in three parts. In the first we analyze the amplitude for the three body interaction corresponding to the box-isospin diagram in fig.3, whose space-time part is given by the set of diagrams in fig.2. In the second part of the paper we consider the cut amplitude and we work out all the leading contribution to the inelastic cross section. A last paragraph is devoted to a final discussion and to a few concluding remarks.

II. Amplitude

This section is divided in two subsections. In sub-section a we make a detailed study of the behavior for large s, fixed t, of the space-time factors of all the diagrams in fig.2. In the following subsection b we discuss the color decomposition of the color factors.

a. *Space-time factors*

In fig.4 one of the diagrams in the set under consideration is shown and the kinematical variables are explicitly indicated. The momentum of the projectile

parton is p_+ and the momenta of the two target partons are $(k_1 - Q)_-$ and $(k_2 + Q)_-$. '+' and '−' are the light-cone frame components which we choose in such a way that the projectile is characterized by values of the '+' momentum component of order $\sqrt{s}$ while the same holds for the '−' momentum components of the target. The typical values of $(k_1)_+$, $(k_2)_+$, $(k_1 - Q)_+$, $(k_2 + Q)_+$ and p_- are of order $m^2/\sqrt{s}$, where m is a typical value for the hadron mass, which gives also the size to the transverse momenta of the external lines. In order to make a meaningful perturbative calculation, we introduce the lower cut-off q_t^{min} for the transverse momenta of the exchanged parton lines q_1, q_2, $q_1 + Q$, $q_2 - Q$, in such a way that $q_t^{min} \gg m$ and $\sqrt{s} \gg q_t^{min}$. As it results from the detailed analysis reported in the next paragraphs, the values for virtuality and transverse momenta, in the dominant loop configurations, are of order q_t^{min}, in the case of the quantities of interest for the present analysis. As a consequence we neglect the virtualities and transverse momenta of the external lines while performing the loop integrals and we threat the lines with momenta p, k_1, k_2, $k_1 - Q$ and $k_2 + Q$ as partons flying in the direction of the parent hadron keeping different from zero only the components p_+, $(k_1)_-$, $(k_2)_-$, $(k_1 - Q)_-$, $(k_2 + Q)_-$ which we take as positive quantities. One may notice that while the target bound state forces the + and transverse components of the corresponding target parton momenta to be small, it allows variations of order $\sqrt{s}$ for the − components. As a consequence values for Q_- of order $\sqrt{s}$ are allowed by the forces which keep the partons in the hadron. Since configurations where the target partons exchange a sizeable longitudinal component Q_- are not damped by the parton wave function, we do not have a genuine forward amplitude and Q_- is one of the variables, in addition to the loop variables, to be integrated over when analyzing the semi-hard interaction. On the other hand the semi-hard interaction, namely the loop integrals, represented in the set of diagrams in fig.2, has a much stronger dependence on Q_- than the bound state. In fact, as it will be seen later, it forces Q_- to be of order $(q_t^{min})^2/\sqrt{s}$. The transverse momenta are constrained by the hadronic bound state to be of order $m \ll q_t^{min}$ and, as a consequence, they must be balanced in the semi-hard interaction, so, with respect to the transverse momenta we have a forward amplitude.

In analogy with ref.3 and ref.4, we write the space-time factors of the diagrams in fig.2 in the Feynman gauge. As discussed in appendix A, to look for the leading contribution we are allowed to neglect the variation of the current couplings at the vertices as a function of the loop variables, in such a way that the loop

integrals involve the denominators of the propagators only. We keep moreover into account that the dominant loop configurations are the ones where the transverse components are small with respect to the c.m. energy[13]. As a consequence, to work out the leading contribution, we treat the transverse components of q_1 and q_2 as small quantities with respect to $\sqrt{s}$.

All the denominators of the propagators in the set of diagrams in fig.2 are numbered below:

$$
\begin{aligned}
a_1 \qquad & (q_2 - Q)^2 = \alpha_2(\beta_2 - \beta_Q)s - q_{2t}^2 + i\epsilon \\
a_2 \qquad & (k_2 + q_2)^2 = \alpha_2(\beta_2 + \beta_{k_2})s - q_{2t}^2 + i\epsilon \\
a_3 \qquad & (q_2)^2 = \alpha_2\beta_2 s - q_{2t}^2 + i\epsilon \\
a_2' \qquad & (k_2 + Q - q_2)^2 = -\alpha_2(\beta_{k_2} - \beta_2 + \beta_Q)s - q_{2t}^2 + i\epsilon \\
a_4 \qquad & (q_1 + Q)^2 = \alpha_1(\beta_1 + \beta_Q)s - q_{1t}^2 + i\epsilon \\
a_5 \qquad & (k_1 + q_1)^2 = \alpha_1(\beta_1 + \beta_{k_1})s - q_{1t}^2 + i\epsilon \\
a_6 \qquad & (q_1)^2 = \alpha_1\beta_1 s - q_{1t}^2 + i\epsilon \\
a_5' \qquad & (k_1 - Q - q_1)^2 = -\alpha_1(\beta_{k_1} - \beta_1 - \beta_Q)s - q_{1t}^2 + i\epsilon \\
a_7 \qquad & (p - q_2 + Q)^2 = (\alpha - \alpha_2)(-\beta_2 + \beta_Q)s - q_{2t}^2 + i\epsilon \\
a_8 \qquad & (p - q_1 - q_2)^2 = (\alpha - \alpha_1 - \alpha_2)(-\beta_1 - \beta_2)s - q_t^2 + i\epsilon \\
a_9 \qquad & (p - q_1)^2 = (\alpha - \alpha_1)(-\beta_1)s - q_{1t}^2 + i\epsilon \\
a_7' \qquad & (p - q_1 - Q)^2 = (\alpha - \alpha_1)(-\beta_1 - \beta_Q)s - q_{1t}^2 + i\epsilon \\
a_9' \qquad & (p - q_2)^2 = (\alpha - \alpha_2)(-\beta_2)s - q_{2t}^2 + i\epsilon \\
a_8' \qquad & (p + Q)^2 = \alpha\beta_Q s + i\epsilon \\
a_8'' \qquad & (p - Q)^2 = \alpha(-\beta_Q)s + i\epsilon
\end{aligned}
$$

where the infinite momentum frame components of the four momenta have been defined as

$$
\begin{aligned}
p \equiv & \sqrt{s}(\alpha, 0, 0) \\
k_{1,2} \equiv & \sqrt{s}(0, \beta_{k_{1,2}}, 0) \\
Q \equiv & \sqrt{s}(0, \beta_Q, 0) \\
q_{1,2} \equiv & \sqrt{s}(\alpha_{1,2}, \beta_{1,2}, \mathbf{q}_{t1,2}/\sqrt{s})
\end{aligned}
$$

and $\mathbf{q}_t$ is defined as $\mathbf{q}_t = \mathbf{q}_{t1} + \mathbf{q}_{t2}$.

One can observe that one may obtain the different topologies in the first column in fig.2 starting from the last diagram, the one numbered 21, whose momenta are explicitly indicated in fig.4, and making the following replacements: $a_7' \to a_7$ to obtain diagram 9, $a_7' \to a_7$ followed by $a_9 \to a_9'$ to obtain 17, $a_9 \to a_9'$ to obtain 13, $a_8 \to a_8'$ and $a_7' \to a_7$ for 1 and $a_8 \to a_8''$ together with $a_9 \to a_9'$ to obtain 5. Moreover one can observe that the set of diagrams in the second column is obtained from the one in the first with the replacement $a_5 \to a_5'$, the third column is obtained replacing a_2 with a_2' and the last one with the substitution $a_2 \to a_2'$ followed by $a_5 \to a_5'$.

To extract the leading contributions, we proceed by analyzing the behavior, for large s and fixed q_t, of the integral of the denominators of the propagators in the two central loops with respect to the longitudinal variables α_1, α_2, β_1, β_2 and β_Q. The integration limits on β_Q are obtained from the positivity requirement for $(k_1 - Q)_-$ and $(k_2 + Q)_-$. In the following however we limit ourselves to consider the region in β_Q where $\beta_Q + \beta_{k_2}$ and $\beta_{k_1} - \beta_Q$ are finite quantities for $q_t^2/s \to 0$. The leading contribution is obtained integrating on α_1, α_2, β_1, β_2 and β_Q the denominators of the propagators and making the limits $q_{t1}^2/s \to 0$, $q_{t2}^2/s \to 0$.

An important point, as far as the integration region providing the leading contribution is concerned, has to be made. Let us consider the sum of three diagrams in fig. 5, which can be considered as a prototype for the whole set. The corresponding integration on the longitudinal variables can be schematically expressed as:

$$\int \frac{1}{a_1 a_2 a_3} \frac{1}{a_7} \left(\frac{1}{a_8' a_9} + \frac{1}{a_8 a_9} + \frac{1}{a_8 a_9'} \right) \frac{1}{a_4 a_5 a_6} \tag{1}$$

The integrations on β_1 and β_2 give the limits for the integrations on α_1 and α_2. We need to recognize the region, in the α_1, α_2 integrations, that provides the dominant term in $1/s$. The region $\alpha_i \approx q_{ti}^2/s$ contributes to the dominant term since six of the denominators in Eq.(1), a_1, a_2, a_3, a_4, a_5, a_6, are of order q_t^2 rather than s. One can notice that, in the case of the diagram III in fig. 5, corresponding to the last term in the sum in Eq.(1), the region $\alpha_1 \approx q_t^2/s$, $\alpha - \alpha_2 \approx q_t^2/s$ gives a contribution of the same order since the denominators a_4, a_5, a_6, a_7, a_8 and a_9' are of order q_t^2 in this case. All different ways of compensating the powers of s in the denominators in Eq.(1) give subleading contributions. The two configurations do

not give a contribution of the same order to the amplitude, as it can be realized when the current structure of the numerators in the propagators is taken into account. In the case $\alpha_i \approx q_{ti}^2/s$, neglecting the terms with $\mathbf{q}_t$, one obtains, for the convective current factors:

$$2p\cdot(2k_2+Q)=\alpha(2\beta_{k_2}+\beta_Q)s \qquad 2p\cdot 2k_2=2\alpha\beta_{k_2}s$$
$$2p\cdot(2k_1-Q)=\alpha(2\beta_{k_1}-\beta_Q)s \qquad 2p\cdot 2k_1=2\alpha\beta_{k_1}s$$

for the diagram I in fig. 5,

$$2p\cdot(2k_2+Q)=\alpha(2\beta_{k_2}+\beta_Q)s \qquad 2p\cdot(2k_1-Q)=\alpha(2\beta_{k_1}-\beta_Q)s$$
$$2p\cdot 2k_2=2\alpha\beta_{k_2}s \qquad 2p\cdot 2k_1=2\alpha\beta_{k_1}s$$

for the diagram II, and

$$2p\cdot(2k_2+Q)=\alpha(2\beta_{k_2}+\beta_Q)s \qquad 2p\cdot(2k_1-Q)=\alpha(2\beta_{k_1}-\beta_Q)s$$
$$2p\cdot 2k_1=2\alpha\beta_{k_1}s \qquad 2p\cdot 2k_2=2\alpha\beta_{k_2}s$$

for the diagram III. For all the three diagrams the leading term in the numerators is given by:

$\alpha^4(2\beta_{k_2}+\beta_Q)(2\beta_{k_1}-\beta_Q)2\beta_{k_1}2\beta_{k_2}s^4$.

In the second case a smaller power of s is obtained from the numerators because of the smallness of the $(p-q_2)_+$ component. For $\alpha_1 \approx q_t^2/s$ and $\alpha-\alpha_2 \approx q_t^2/s$ the current couplings associated with the 'p' line in the diagram III in fig.5 are: $p\cdot(2k_2+Q)=\alpha(\beta_{k_2}+\beta_Q/2)s$, $\mathrm{O}(q_t\sqrt{s})$, $\mathrm{O}(q_t\sqrt{s})$ and $p\cdot 2k_2=\alpha\beta_{k_2}s$.
As a consequence this case is suppressed by at least one power of s with respect to the previous one.

When considering the cut diagrams the leading contribution is analogously obtained from the region $\alpha_i \approx q_t^2/s$, as we have explicitly verified. We proceed considering separately all the 24 diagrams in fig.2, limiting the analysis to the dominant integration region.

The set of 24 diagrams can be divided in three different sub-sets with the different topologies of the three diagrams in fig.5. Diagram I is the prototype for the first eight diagrams in fig.2, diagram II is the prototype for the diagrams $9-16$ and diagram III is the prototype for the last $17-24$. We call $\mathcal{M}_i$ the integrations on α_1, α_2, β_1, β_2 and β_Q of the denominators corresponding to the ith diagram in fig.2. Each one of the eight diagrams of the kind of diagram I in

fig.5 gives a negligible contribution in the limit under consideration. In fact let us evaluate explicitly $\mathcal{M}_1$: The leading term corresponding to the three denominators associated with the projectile is:

$$\left(\frac{1}{a_7 a_8' a_9}\right) = \frac{1}{\alpha^3 s^3} \frac{1}{(-\beta_2 + \beta_Q + i\epsilon)(\beta_Q + i\epsilon)(-\beta_1 + i\epsilon)} \tag{2}$$

the integrations involve also the denominators of the exchanged partons a_1, a_3, a_4 and a_6. A discussion on some subleading terms is presented in appendix **B**. The dependence of a_2 and a_5 on the contrary can be neglected when considering the dominant integration region. The integral on β_1 can be done taking the residuum of the pole $1/a_9$, which gives $\beta_1 = 0$ and forces the condition $\alpha_1 > 0$. Analogously the integral on β_2 gives $\beta_2 = \beta_Q$ with $\alpha_2 > 0$. All the poles which are left for the integration on β_Q are listed below:

$$\begin{aligned}
a_1 &= -q_{2t}^2 \\
a_3 &= \alpha_2 \beta_Q s - q_{2t}^2 + i\epsilon \\
a_4 &= \alpha_1 \beta_Q s - q_{1t}^2 + i\epsilon \\
a_6 &= -q_{1t}^2 \\
a_8' &= \alpha \beta_Q s + i\epsilon
\end{aligned}$$

and one can notice that the conditions $\alpha_1 > 0$ and $\alpha_2 > 0$ force all singularities on the same size in the complex β_Q plane. One obtains therefore zero, in fact this is a particular case where the A.F.S. cancellation[14] applies. A similar argument holds for all the first eight diagrams in fig.2.

Each one of the diagrams of the set II gives a contribution of order $\ln s$. Let us consider explicitly the case of diagram II in fig.5. The leading term corresponding to the three denominators associated with the projectile is:

$$\left(\frac{1}{a_7 a_8 a_9}\right) = \frac{1}{\alpha^3 s^3} \frac{1}{(-\beta_2 + \beta_Q + i\epsilon)(-\beta_1 - \beta_2 + i\epsilon)(-\beta_1 + i\epsilon)} \tag{3}$$

The integrations on β_1, β_2 and β_Q involve also the vertical propagators with denominators a_1, a_3, a_4, a_6. To obtain a result different from zero from the integrations on β_1 and β_2 one needs to have $\alpha_1 > 0$ and $\alpha_2 > 0$. The integration on β_Q is done by taking the residuum of the pole $1/a_1$. The integration on β_2 with the pole $1/a_8$ and the integration on β_1 with the pole $1/a_6$. The integral on the longitudinal variables α_1 and α_2 is therefore expressed as

$$\mathcal{M}_9 = \frac{-(2\pi i)^3}{\alpha^3 s^3} \int_{\substack{\alpha_1>0 \\ \alpha_2>0}} \frac{\alpha_1 \alpha_2 d\alpha_1 d\alpha_2}{q_{1t}^2 q_{2t}^2 (\alpha_2 q_{1t}^2 + \alpha_1 q_{2t}^2)^2 a_5 a_2} \tag{4}$$

The same expression is obtained for $\mathcal{M}_{12}$, $\mathcal{M}_{13}$ and $\mathcal{M}_{16}$. The integration domain in α_1 and α_2 is different however:

$$\mathcal{M}_{12} : \{\alpha_1 < 0, \alpha_2 < 0\}$$
$$\mathcal{M}_{13} : \{\alpha_1 > 0, \alpha_2 > 0\}$$
$$\mathcal{M}_{16} : \{\alpha_1 < 0, \alpha_2 < 0\}$$

When considering $\mathcal{M}_{10}$, $\mathcal{M}_{11}$, $\mathcal{M}_{14}$ and $\mathcal{M}_{15}$ one obtains:

$$\frac{(2\pi i)^3}{\alpha^3 s^3} \int \frac{\alpha_1 \alpha_2 d\alpha_1 d\alpha_2}{q_{1t}^2 q_{2t}^2 (\alpha_2 q_{1t}^2 - \alpha_1 q_{2t}^2)^2 a_5 a_2} \tag{5}$$

and the corresponding integration domains are

$$\mathcal{M}_{10} : \{\alpha_1 < 0, \alpha_2 > 0\}$$
$$\mathcal{M}_{11} : \{\alpha_1 > 0, \alpha_2 < 0\}$$
$$\mathcal{M}_{14} : \{\alpha_1 < 0, \alpha_2 > 0\}$$
$$\mathcal{M}_{15} : \{\alpha_1 > 0, \alpha_2 < 0\}$$

A closer look to the integrals in Eq.(4) and in Eq.(5) shows that they both give rise to a $\ln s$ factor which is originated from the integration region $\alpha_1 \propto \alpha_2 \to 0$.

The last eight diagrams in fig.2 are leading, namely they are of order $(\ln s)^2$. Let us consider the diagram *III* in fig.5: The leading term corresponding to the three denominators associated with the projectile is:

$$\left(\frac{1}{a_7 a_8 a_9'}\right) = \frac{1}{\alpha^3 s^3} \frac{1}{(-\beta_2 + \beta_Q + i\epsilon)(-\beta_1 - \beta_2 + i\epsilon)(-\beta_2 + i\epsilon)} \tag{6}$$

to integrate on β_1, β_2 and β_Q one needs to consider also the vertical propagators with denominators a_1, a_3, a_4, a_6. As in the previous cases, to obtain a result different from zero from the integrations on β_1 and β_2, one needs to have $\alpha_1 > 0$ and $\alpha_2 > 0$. One may integrate on β_Q with the pole $1/a_1$, on β_1 with the pole $1/a_8$ and on β_2 with the pole $1/a_3$. $\mathcal{M}_{17}$ is then given by:

$$\mathcal{M}_{17} = \frac{-(2\pi i)^3}{\alpha^3 s^3} \int_{\substack{\alpha_1>0 \\ \alpha_2>0}} \frac{\alpha_2^2 d\alpha_1 d\alpha_2}{(q_{2t}^2)^2 (\alpha_2 q_{1t}^2 + \alpha_1 q_{2t}^2)^2 a_5 a_2} \tag{7}$$

The same expression is obtained for $\mathcal{M}_{20}$, with the integration domain however replaced by $\alpha_1 < 0$, $\alpha_2 < 0$. $\mathcal{M}_{21}$ and $\mathcal{M}_{24}$ give:

$$\frac{-(2\pi i)^3}{\alpha^3 s^3} \int \frac{\alpha_1^2 d\alpha_1 d\alpha_2}{(q_{1t}^2)^2(\alpha_2 q_{1t}^2 + \alpha_1 q_{2t}^2)^2 a_5 a_2} \tag{8}$$

with the integration limits

$$\mathcal{M}_{21} : \{\alpha_1 > 0, \alpha_2 > 0\}$$
$$\mathcal{M}_{24} : \{\alpha_1 < 0, \alpha_2 < 0\}$$

For $\mathcal{M}_{18}$ and $\mathcal{M}_{19}$ one obtains:

$$\frac{-(2\pi i)^3}{\alpha^3 s^3} \int \frac{\alpha_2^2 d\alpha_1 d\alpha_2}{(q_{2t}^2)^2(\alpha_2 q_{1t}^2 - \alpha_1 q_{2t}^2)^2 a_5 a_2} \tag{9}$$

with

$$\mathcal{M}_{18} : \{\alpha_1 < 0, \alpha_2 > 0\}$$
$$\mathcal{M}_{19} : \{\alpha_1 > 0, \alpha_2 < 0\}$$

Finally $\mathcal{M}_{22}$ and $\mathcal{M}_{23}$:

$$\frac{-(2\pi i)^3}{\alpha^3 s^3} \int \frac{\alpha_1^2 d\alpha_1 d\alpha_2}{(q_{1t}^2)^2(\alpha_2 q_{1t}^2 - \alpha_1 q_{2t}^2)^2 a_5 a_2} \tag{10}$$

with

$$\mathcal{M}_{22} : \{\alpha_1 < 0, \alpha_2 > 0\}$$
$$\mathcal{M}_{23} : \{\alpha_1 > 0, \alpha_2 < 0\}$$

In all cases a factor $(\ln s)^2$ is obtained, in Eq.(7) and in Eq.(9) from the region $|\alpha_1| \ll |\alpha_2| \to 0$, while in Eq.(8) and in Eq.(10) from the region $|\alpha_2| \ll |\alpha_1| \to 0$. As a consequence the leading behavior for all the diagrams of the set *III* is obtained from the same integral

$$\frac{-(2\pi i)^3}{\alpha^3 s^3} \frac{1}{(q_{1t}^2)^2 (q_{2t}^2)^2} \int \frac{d\alpha_1 d\alpha_2}{a_5 a_2} \tag{11}$$

in the region $|\alpha_1| \to 0$, $|\alpha_2| \to 0$, with the constraints on the signs of α_1 and α_2 just mentioned. The sign of the leading log in every $\mathcal{M}$ is obtained by looking to the corresponding different cuts, in the α_1-α_2 plane, representing the integration

limits, for small $|\alpha_1|$, $|\alpha_2|$, of the integral in Eq.(11). The leading term, at large s, for $\mathcal{M}_{17}$, $\mathcal{M}_{20}$, $\mathcal{M}_{21}$ and $\mathcal{M}_{24}$ is expressed as

$$\frac{(-2\pi i)^3}{\alpha^3 \beta_{k_1} \beta_{k_2} (q_{1t}^2)^2 (q_{2t}^2)^2} (\ln s)^2$$

while for $\mathcal{M}_{18}$, $\mathcal{M}_{19}$, $\mathcal{M}_{22}$ and $\mathcal{M}_{23}$ one obtains the same with opposite sign. One may notice that, although each single term is of order $(\ln s)^2$, when summing two terms, with contiguous integration regions, like $\mathcal{M}_{22} + \mathcal{M}_{24}$, corresponding to $\{\alpha_1 < 0, \alpha_2 > 0\} \cup \{\alpha_1 < 0, \alpha_2 < 0\} \equiv \{\alpha_1 < 0\}$, one obtains a leading behavior which is of order $\ln s$ rather than $(\ln s)^2$. In the case just mentioned the $\ln s$ factor is obtained as a result of the integration limit for α_1. The integration on α_2 does not produce any more a further $\ln s$, since, in the integrand $1/a_2$, the configurations with α_2 small and negative compensate the ones with α_2 small and positive.

b. *Color decomposition*

The lowest order contribution to the isospin diagram in fig.3 is selected by looking at the quantum numbers. The projectile parton exchanges four gluons and each of the target partons two gluons, moreover the lowest order in the coupling constant g is eight. The set in fig.2 is the complete set of diagrams fulfilling these conditions. The color factors in the set of diagrams in fig.2 however contain also the exchanges of a color octet in one and also in both t-channels. The purpose of the present paragraph is to gain a better understanding of the color structure of the amplitude corresponding to the set of diagrams in fig.2. More precisely we would like to recover, in this three body interaction case, a collocation for the logs, obtained from the single Feynman diagrams in fig.2, which is consistent with the general features encountered when discussing gluon Reggeization in the two body interaction.

We need to analyze the 16 diagrams of the sub-sets II and III, corresponding to the diagrams $9 - 24$ in fig.2. The diagrams $1 - 8$ in fig.2, corresponding to the sub-set I, give a negligible contribution in the high energy limit. There are 16 color factors T_i, $i = 9 \ldots 24$, which are identified by the topology of the 16 diagrams of interest. On the other hand we are interested in identifying the components of the color factors which correspond to the exchange of a single gluon in each of the t-channels. To that purpose we use the graphical representation of the

commutation relations, for the color matrices representing the couplings with the exchanged gluons, as shown in fig.6. The 16 color factors T_i, $i = 9 \ldots 24$, are then expressed as linear combinations of the 16 color factors G_i, $i = 1 \ldots 16$, shown in fig.7. We consider separately the two different sub-sets II and III. Let us start with the diagrams in the sub-set III which are characterized by a $(\ln s)^2$ factor.

$$\begin{aligned}
T_{17} =& G_1 + G_3 - G_2 \\
T_{18} =& G_1 + G_3 - G_2 - G_8 \\
T_{19} =& G_1 + G_3 - G_2 + G_6 \\
T_{20} =& G_1 + G_3 - G_2 - G_8 + G_6 - G_{14} \\
T_{21} =& G_1 \\
T_{22} =& G_1 - G_5 \\
T_{23} =& G_1 + G_7 \\
T_{24} =& G_1 - G_5 + G_7 - G_{13}
\end{aligned} \tag{12}$$

The eight relations in Eq.(12) can be inverted and the amplitude M_{III} corresponding to the set of diagrams III in fig.5 can be expressed as a sum of terms with color factors G:

$$\begin{aligned}
M_{III} =& G_1 \times \sum_{i=17}^{24} \mathcal{M}_i + (G_3 - G_2) \times \sum_{i=17}^{20} \mathcal{M}_i \\
&+ G_6 \times (\mathcal{M}_{19} + \mathcal{M}_{20}) - G_5 \times (\mathcal{M}_{22} + \mathcal{M}_{24}) \\
&+ G_7 \times (\mathcal{M}_{23} + \mathcal{M}_{24}) - G_8 \times (\mathcal{M}_{18} + \mathcal{M}_{20}) \\
&- G_{13} \times \mathcal{M}_{24} - G_{14} \times \mathcal{M}_{20}
\end{aligned} \tag{13}$$

It is interesting to notice that, while each of the space-time factors $\mathcal{M}$ is separately of order $(\ln s)^2$, the sum of different $\mathcal{M}$'s can be of order $\ln s$, or even it can be a constant, due to the different signs going with the logs in the different terms. The behavior of the space-time factors in Eq.(13) is obtained as discussed in the previous paragraph. The result is the following: there is no $\ln s$ in the space-time factor multiplying G_1 and $G_3 - G_2$, on the contrary G_5, G_6, G_7 and G_8 multiply a space-time factor of order $\ln s$ and, obviously, G_{13} and G_{14} multiply a $(\ln s)^2$. One may further notice that, if one considers the simplest case where the colors of the two target partons are summed independently, one trivially obtains that G_5, G_6, G_7, G_8, G_{13} and G_{14} are all zero. The sum $G_3 - G_2$ is also zero, even if G_3 and

G_2 are separately different from zero. G_1, which is precisely the color factor in fig.3, is the only color factor which remains finite.

A similar decomposition can be done for the color factors of the diagrams in the set II:

$$\begin{aligned}
T_9 =& G_1 + G_3 + G_4 \\
T_{10} =& G_1 + G_3 + G_4 - G_{10} \\
T_{11} =& G_1 + G_3 + G_4 + G_9 \\
T_{12} =& G_1 + G_3 + G_4 + G_9 - G_{10} - G_{15} \\
T_{13} =& G_1 - G_2 \\
T_{14} =& G_1 - G_2 - G_{12} \\
T_{15} =& G_1 - G_2 + G_{11} \\
T_{16} =& G_1 - G_2 + G_{11} - G_{12} - G_{16}
\end{aligned} \tag{14}$$

The corresponding amplitude M_{II} is therefore expressed as:

$$\begin{aligned}
M_{II} =& G_1 \times \sum_{i=9}^{16} \mathcal{M}_i + (G_3 + G_4) \times \sum_{i=9}^{12} \mathcal{M}_i - G_2 \times \sum_{i=13}^{16} \mathcal{M}_i \\
&+ G_9 \times (\mathcal{M}_{11} + \mathcal{M}_{12}) - G_{10} \times (\mathcal{M}_{10} + \mathcal{M}_{12}) \\
&+ G_{11} \times (\mathcal{M}_{15} + \mathcal{M}_{16}) - G_{12} \times (\mathcal{M}_{14} + \mathcal{M}_{16}) \\
&- G_{15} \times \mathcal{M}_{12} - G_{16} \times \mathcal{M}_{16}
\end{aligned} \tag{15}$$

There are no more space-time factors of order $\ln s$ in Eq.(15), with the obvious exception of $\mathcal{M}_{12}$ and $\mathcal{M}_{16}$, which multiply G_{15} and G_{16} respectively. When summing on the two colors of the target partons independently, in order to remove all color factors which contain the exchange of a single gluon in at least one of the two t-channels, G_9, G_{10}, G_{11}, G_{12}, G_{15} and G_{16} are trivially zero. G_3 and G_2 are opposite in sign, while the leading term in the corresponding space-time factors are equal. G_1 and G_4 are the only color factors which contribute.

As a summary, the amplitude corresponding to the sum of the Feynman diagrams in fig.2 can be written, for $s \to \infty$, $t/s \to 0$, as $M_{III} + M_{II}$, with M_{III} and M_{II} expressed, as in Eq.(13) and in Eq.(15), by means of a sum of terms with the color factors G_i, $i = 1 \ldots 16$, shown in fig.7. Two color factors, G_{13} and G_{14}, multiply a term of order $(\ln s)^2$. G_{13} and G_{14}, using the rules for the isospin diagrams discussed in the case of the two body interaction[3,4], are readily shown to

be proportional to the base-isospin diagram of order g^4, which corresponds to the exchange of one gluon in each of the two t-channels. The $(g^2 \ln s)^2$ in the space-time factor is therefore understood as a contribution to the Reggeization of the two gluons exchanged in the lowest order g^4 base-isospin diagram. G_5, G_6, G_7, G_8, G_{15} and G_{16} multiply space-time factors of order $\ln s$. They all contain the exchange of a color octet in at least one of the two t-channels. The corresponding amplitude contains both corrections of order $g^2 \ln s$ to base-isospin diagrams of order g^6, associated with the eikonal diagrams at the same order, and further isospin diagrams at order g^8 of kind b, which, in analogy with the case of the two body interaction, are expected to contain a $\ln s$ factor already at the lowest order. All terms with logs can find a collocation consistent with the analysis of the two-body interaction, and, at this order, contain octet quantum number exchanges. To project out the case of interest, which is characterized by vacuum quantum number exchange, we sum the colors of the two target partons independently. All exchanges of color octets are then zero. The color factors which are selected in this way are G_1, G_2, G_3 and G_4. G_2 and G_3 multiply a space-time factor which is suppressed as a power of $(q_t^{min})^2/s$ with respect to the leading term. G_1 and G_4 are the only color factors with exchange of vacuum quantum numbers multiplying a space-time factor which is not suppressed. G_4, corresponding to the exchange of two gluons by the projectile parton, does receive contributions by a whole set of further diagrams, in addition to the set of diagrams in fig.2, and is not studied in the present paper. G_1, which is the isospin diagram already shown in fig.3, receives contributions, at order g^8, by the set of Feynman diagrams in fig.2 only.

III. Cut amplitude

In this part of the paper we study the cuts of the amplitude corresponding to the set of diagrams in fig.2. Although some cut-diagrams are zero, in the limit of interest, we find convenient to include them too in the discussion. The reason is that the evaluation of the sum of all the eikonal diagrams, contributing to the same cut amplitude, is simpler than the evaluation of each single cut diagram separately. This section is organized in three different sub-sections, in accordance with the three different kinds of cuts to be considered.

III.1 Two box cuts, *Case* a

In the present sub-section we analyze all cuts where both interactions of the projectile with the target partons are involved. We start with the observation that the mass shell constraint on the external lines, together with the requirement $q_t \geq q_t^{min}$ is greatly reduces the number of possible cuts. In fact, for example, the case in the diagram of fig.4, where the lines with momenta $q_1 + Q_-$ and $p_+ - Q_- - q_1$ are cut, is not allowed. In fact, in this case, the invariant mass of p is forced to be of order $q_t > q_t^{min} \gg m$, which is the scale for the virtuality of all the external lines. All allowed cuts, where both target partons are involved, are of the three different kinds shown in fig. 8.

As a first case we consider the cuts of the kind in fig. 8*a* (*case* a), where the lines identified by a_2, a_8 and a_5 are cut. Only the four cut diagrams in fig.9 contribute. The mass shell conditions for the cut lines are:

$$\begin{aligned} a_2 &= \alpha_2(\beta_2 + \beta_{k_2})s - q_{2t}^2 = 0 \\ a_5 &= \alpha_1(\beta_1 + \beta_{k_1})s - q_{1t}^2 = 0 \\ a_8 &= (\alpha - \alpha_1 - \alpha_2)(-\beta_1 - \beta_2)s - q_t^2 = 0, \end{aligned} \tag{16}$$

the condition of positivity for the energies of the cut parton lines is:

$$\begin{aligned} &\alpha_2 + \beta_2 + \beta_{k_2} \geq 0 \\ &\alpha_1 + \beta_1 + \beta_{k_1} \geq 0 \\ &\alpha - \alpha_1 - \alpha_2 - \beta_1 - \beta_2 \geq 0 \end{aligned} \tag{17}$$

and the denominators to be integrated can be written as:

$$\begin{aligned}
a_1 \quad & (q_2 - Q)^2 = -\alpha_2(\beta_{k_2} + \beta_Q)s \\
a_3 \quad & (q_2)^2 = -\alpha_2\beta_{k_2}s \\
a_4 \quad & (q_1 + Q)^2 = -\alpha_1(\beta_{k_1} - \beta_Q)s \\
a_6 \quad & (q_1)^2 = -\alpha_1\beta_{k_1}s \\
a_7 \quad & (p - q_2 + Q)^2 = \alpha(-\beta_2 + \beta_Q)s - \alpha_2(\beta_{k_2} + \beta_Q)s + i\epsilon \\
a_9 \quad & (p - q_1)^2 = -\alpha\beta_1 s - \alpha_1\beta_{k_1}s + i\epsilon \\
a_7' \quad & (p - q_1 - Q)^2 = -\alpha(\beta_1 + \beta_Q)s - \alpha_1(\beta_{k_1} - \beta_Q)s + i\epsilon \\
a_9' \quad & (p - q_2)^2 = -\alpha\beta_2 s - \alpha_2\beta_{k_2}s + i\epsilon.
\end{aligned}$$

The following expression represents the integration of interest, on the longitudinal variables α_1, α_2, β_1, β_2 and β_Q, corresponding to the four graphs in fig.9.

$$\int \frac{1}{a_1 a_3 a_4 a_6}\Big(\frac{1}{a_7}+\frac{1}{a_7'}\Big)\Big(\frac{1}{a_9}+\frac{1}{a_9'}\Big)\delta(a_2)\delta(a_8)\delta(a_5). \tag{18}$$

The leading terms is obtained when $\alpha_i \approx q_t^2/s$. The solution of interest for the mass shell conditions, Eq.(16), is then:

$$\begin{aligned} \alpha_1 &\simeq \frac{q_{1t}^2}{(\beta+\beta_{k_1})s} \\ \alpha_2 &\simeq \frac{q_{2t}^2}{(-\beta+\beta_{k_2})s} \\ B &\simeq \frac{-q_t^2}{\alpha s} \end{aligned} \tag{19}$$

where terms of higher order in q_t^2/s have been neglected, $\beta_1 = \beta + B/2$, $\beta_2 = -\beta + B/2$ and both $\beta+\beta_{k_1}$ and $-\beta+\beta_{k_2}$ are finite quantities in the limit $q_t^2/s \to 0$. The integrations on α_1, α_2 and B are done with the help of the δ-functions and Eq.(18) reduces to:

$$\begin{aligned} \int \frac{d\beta d\beta_Q}{\beta_{k_1}\beta_{k_2}\alpha(q_{t1}^2)^2(q_{t2}^2)^2 s^3}\frac{(\beta_{k_1}+\beta)(\beta_{k_2}-\beta)}{(\beta_{k_1}-\beta_Q)(\beta_{k_2}+\beta_Q)} \\ \times\Bigg\{\frac{1}{\alpha(\beta+\beta_Q)s+\frac{q_t^2}{2}-q_{t2}^2\frac{\beta_{k_2}+\beta_Q}{\beta_{k_2}-\beta}+i\epsilon} \\ +\frac{1}{-\alpha(\beta+\beta_Q)s+\frac{q_t^2}{2}-q_{t1}^2\frac{\beta_{k_1}-\beta_Q}{\beta_{k_1}+\beta}+i\epsilon}\Bigg\} \\ \times\Bigg\{\frac{1}{-\alpha\beta s+\frac{q_t^2}{2}-q_{t1}^2\frac{\beta_{k_1}}{\beta_{k_1}+\beta}+i\epsilon} \\ +\frac{1}{\alpha\beta s+\frac{q_t^2}{2}-q_{t2}^2\frac{\beta_{k_2}}{\beta_{k_2}-\beta}+i\epsilon}\Bigg\} \end{aligned} \tag{20}$$

The integration limits for β_Q are a consequence of the constraint of positivity for $(k_1-Q)_-$ and $(k_2+Q)_-$, the limits for β come from the condition of positivity of the cut parton lines, Eq.(17). The leading contribution is readily obtained after noticing that the contribution to the integral from the region where $(\beta+\beta_Q)$

is finite is suppressed as a power of q_t^2/s, for large values of s, because of the cancellation between $1/a_7$ and $1/a_7'$:

$$\left(\frac{1}{a_7}+\frac{1}{a_7'}\right)\to\frac{1}{\alpha(\beta+\beta_Q)s}+\frac{1}{-\alpha(\beta+\beta_Q)s}+\mathcal{O}\left(\frac{q_t^2}{s^2}\right)$$

The same cancellation occurs, when β is finite, in the factor $\left(1/a_9+1/a_9'\right)$. To obtain the leading term we are therefore allowed to integrate over β_Q keeping track of the dependence on β_Q only in the terms proportional to s in a_7 and a_7', while we can integrate on β keeping the dependence on β only in the terms proportional to s in a_9 and a_9'. More explicitly, the actual integral on β_Q (in a region of size of order q_t^2/s around $\beta_Q=\beta$) is:

$$\int d\beta_Q\left(\frac{1}{\alpha(\beta+\beta_Q)s+\frac{1}{2}q_t^2-q_{t2}^2+i\epsilon}+\frac{1}{-\alpha(\beta+\beta_Q)s+\frac{1}{2}q_t^2-q_{t1}^2+i\epsilon}\right)$$

If one replaces $\mathbf{q}_{t1}$ with $-\mathbf{q}_{t1}$ in the second integral, the second term is the opposite of the complex conjugate of the first. One is then allowed to replace the sum of the two integrals with a single integral, involving the first integrand only, performed along a closed contour, in the complex β_Q plane, including the polar singularity of $1/a_7$:

$$\int d\beta_Q\left(\frac{1}{\alpha(\beta+\beta_Q)s-a+i\epsilon}+\frac{1}{-\alpha(\beta+\beta_Q)s+a+i\epsilon}\right)=\oint\frac{d\beta_Q}{\alpha(\beta+\beta_Q)s-a}$$

where $a=q_t^2/2-q_{t1}^2$. The integration over β_Q is providing a factor $2i\pi/\alpha s$ as a result. The integration on β, that involves (as a leading contribution) the factor $\left(1/a_9+1/a_9'\right)$ only, is done, with the same line of arguments, in a region of β of size of order q_t^2/s around zero. The resulting leading contribution from the configuration with α_1, α_2 and $\beta_1+\beta_2$ of order q_t^2/s is expresses as:

$$\frac{(2\pi)^5}{\beta_{k_1}\beta_{k_2}\alpha^3 s^5}\frac{1}{(q_{t1}^2)^2(q_{t2}^2)^2}. \tag{21}$$

The result which has been obtained is proportional to the product of two elementary partonic cross sections. In fact this term is evaluated by squaring two successive interaction amplitudes between on shell partons. The intermediate partons are put on shell as a result of the contribution to the cross section from the

pinch singularities produced from the constructive interferences between $1/a_7$ and $1/a_7'$, when performing the β_Q integration, and between $1/a_9$ and $1/a_9'$ in the case of the integral on β.

The mass shell conditions, Eq.(16), can be solved differently. In the limit $q_t^2/s \to 0$ one finds a set of six different solutions:

$$\left\{\begin{array}{lll} \alpha_2 \approx 0, & \alpha_1 \approx 0, & \beta_1+\beta_2 \approx 0; \\ \alpha_2 \approx 0, & \beta_1+\beta_{k_1} \approx 0, & \alpha_1-\alpha \approx 0; \\ \alpha_2 \approx 0, & \beta_1+\beta_{k_1} \approx 0, & \beta_2-\beta_{k_1} \approx 0; \\ \beta_2+\beta_{k_2} \approx 0, & \beta_1+\beta_{k_1} \approx 0, & \alpha-\alpha_1-\alpha_2 \approx 0; \\ \beta_2+\beta_{k_2} \approx 0, & \alpha_1 \approx 0, & \alpha-\alpha_2 \approx 0; \\ \beta_2+\beta_{k_2} \approx 0, & \alpha_1 \approx 0, & \beta_1-\beta_{k_2} \approx 0; \end{array}\right. \tag{22}$$

where ≈ 0 means $= \mathcal{O}(q_t^2/s)$. For all different solutions, with the exception of the first one, that has been discussed previously, α_1 or α_2 are finite in the $q_t^2/s \to 0$ limit and, analogously to the uncut graph, the corresponding contribution is a subleading one.

Cases **b** *and* **c**

The second case we consider is that one of the cuts of kind in fig.8*b* (*case* **b**). The set of cut diagrams that we have analyzed is represented in fig.10. Altogether there are four sets of diagrams of this kind. They are obtained from the set that we have considered moving, in each diagram, the cut from a_3 to a_1, exchanging the top with the bottom and combining the two operations. Each set of diagrams gives the same contribution.

The difference with respect to the previous case is that the parton lines that are cut are presently identified by a_1, a_8 and a_5. The mass shell conditions are:

$$\begin{aligned} a_1 &= \alpha_2(\beta_2-\beta_Q)s - q_{2t}^2 = 0 \\ a_5 &= \alpha_1(\beta_1+\beta_{k_1})s - q_{1t}^2 = 0 \\ a_8 &= (\alpha-\alpha_1-\alpha_2)(-\beta_1-\beta_2)s - q_t^2 = 0, \end{aligned} \tag{23}$$

the condition of positivity for the energies of the cut parton lines is:

$$\begin{aligned} &\alpha_2+\beta_2-\beta_Q \geq 0 \\ &\alpha_1+\beta_1+\beta_{k_1} \geq 0 \\ &\alpha-\alpha_1-\alpha_2-\beta_1-\beta_2 \geq 0 \end{aligned} \tag{24}$$

and the denominators to be integrated become:

$$
\begin{aligned}
a_2 \qquad & (k_2+q_2)^2 = \alpha_2(\beta_Q+\beta_{k_2})s + i\epsilon \\
a_3 \qquad & (q_2)^2 = \alpha_2\beta_Q s + i\epsilon \\
a_2' \qquad & (k_2+Q-q_2)^2 = -\alpha_2\beta_{k_2}s + i\epsilon \\
a_4 \qquad & (q_1+Q)^2 = \alpha_1(-\beta_{k_1}+\beta_Q)s \\
a_6 \qquad & (q_1)^2 = -\alpha_1\beta_{k_1}s \\
a_7 \qquad & (p-q_2+Q)^2 = \alpha(-\beta_2+\beta_Q)s \\
a_9 \qquad & (p-q_1)^2 = -\alpha\beta_1 s - \alpha_1\beta_{k_1}s + i\epsilon \\
a_7' \qquad & (p-q_1-Q)^2 = -\alpha(\beta_1+\beta_Q)s - \alpha_1(\beta_{k_1}-\beta_Q)s \\
a_9' \qquad & (p-q_2)^2 = -\alpha\beta_2 s + \alpha_2\beta_Q s + i\epsilon.
\end{aligned}
$$

The integrations on the longitudinal variables α_1, α_2, β_1, β_2 and β_Q, corresponding to the graphs in fig.10, is expressed as:

$$
\int \frac{1}{a_3 a_4 a_6}\Big(\frac{1}{a_2}+\frac{1}{a_2'}\Big)\Big(\frac{1}{a_7}+\frac{1}{a_7'}\Big)\Big(\frac{1}{a_9}+\frac{1}{a_9'}\Big)\delta(a_1)\delta(a_8)\delta(a_5). \tag{25}
$$

The mass shell conditions, in the limit $q_t^2/s \to 0$, give rise to the set of possible configurations:

$$
\begin{cases}
\alpha_2 \approx 0, & \alpha_1 \approx 0, & \beta_1+\beta_2 \approx 0; \\
\alpha_2 \approx 0, & \beta_1+\beta_{k_1} \approx 0, & \alpha_1-\alpha \approx 0; \\
\alpha_2 \approx 0, & \beta_1+\beta_{k_1} \approx 0, & \beta_2-\beta_{k_1} \approx 0; \\
\beta_2-\beta_Q \approx 0, & \beta_1+\beta_{k_1} \approx 0, & \alpha-\alpha_1-\alpha_2 \approx 0; \\
\beta_2-\beta_Q \approx 0, & \alpha_1 \approx 0, & \alpha-\alpha_2 \approx 0; \\
\beta_2-\beta_Q \approx 0, & \alpha_1 \approx 0, & \beta_1+\beta_Q \approx 0;
\end{cases} \tag{26}
$$

(where ≈ 0 means $= \mathcal{O}(q_t^2/s)$). The most important contributions are obtained, in the configuration α_2, $\beta_1+\beta_{k_1}$ and $\alpha-\alpha_1 = \mathcal{O}(q_t^2/s)$, by the combination:

$$
\int\Big(\frac{1}{a_2}+\frac{1}{a_2'}\Big)\frac{1}{a_3 a_4 a_6 a_7' a_9}\delta(a_1)\delta(a_8)\delta(a_5) = \mathcal{O}\Big(\frac{1}{(q_t^2)^4}\frac{1}{s^5}\Big) \tag{27}
$$

and in the configuration α_1, $\beta_2-\beta_Q$ and $\beta_1+\beta_Q = \mathcal{O}(q_t^2/s)$ by:

$$
\int\Big(\frac{1}{a_2}+\frac{1}{a_2'}\Big)\frac{1}{a_3 a_4 a_6 a_7 a_9'}\delta(a_1)\delta(a_8)\delta(a_5) = \mathcal{O}\Big(\frac{1}{(q_t^2)^4}\frac{1}{s^5}\Big) \tag{28}
$$

giving rise, however, to non leading terms, after taking into account the numerators in the propagators. The configuration α_1, α_2, $\beta_1 + \beta_2 = \mathcal{O}(q_t^2/s)$ that, in *case* a, gives the leading contribution, is depressed as a power of q_t^2/s with respect to the leading term in the present case: In fact, the mass shell conditions, Eq.(23), force the coefficients of the terms in s of a_7 and a_7' to be $\neq 0$ and opposite in sign while the condition $\alpha_2 = \mathcal{O}(q_t^2/s)$ forces $\beta + \beta_Q \neq \mathcal{O}(q_t^2/s)$, where $\beta = (\beta_1 - \beta_2)/2$. As a consequence the factor $(1/a_7 + 1/a_7')$ is of order (q_t^2/s^2). While in *case* a the conditions of reality for the cut lines where allowing a_7 and a_7' to go on shell, this is not possible any more with the present cuts. The consequence is that in *case* b there is no pinch singularity, corresponding to the sum of the imaginary parts of a_7 and a_7', only the real parts are left that interfere destructively providing the extra suppression factor.

Things are qualitatively analogous to *case* b when considering *case* c, corresponding to the cuts of kind shown in fig.8*c*. More precisely all cuts of this kind are those represented in fig.11 and those obtained exchanging the top with the bottom in each of the graphs in fig.11. The most important contribution (that however does not contribute to the leading term) comes from the set of graphs in fig.11*a* in correspondence with the configuration α_1, $\beta_2 - \beta_Q$ and $\alpha - \alpha_2$ of order q_t^2/s and from those in fig.11*b* in correspondence with the configuration β_1, α_2 and $\alpha - \alpha_1$ of order q_t^2/s. The configuration α_1, α_2 and $\beta_1 + \beta_2$ of order q_t^2/s is now depressed as $(q_t^2/s)^2$ with respect to the leading because the conditions of reality for the cut parton lines force $1/a_7$ and $1/a_7'$ as well as $1/a_9$ and $1/a_9'$ to interfere destructively.

III.2 One box cuts, *case* a

In this section we analyze the cuts where one of the two target partons acts as a spectator. There are two different kinds of cuts to be considered, the first case is that one where two horizontal lines are cut (*case* a), the second is the case where the cut involves one horizontal and one vertical line (*case* b).

The cut diagrams of *case* a that we consider are shown in fig.12. All possible cuts of this kind are four times as many, corresponding to the four independent possibilities of choosing the vertical lines to be cut. Each different set of cut diagrams is providing the same contribution as the set we are considering. Our result has then to be multiplied by four to account for this multiplicity factor.

The mass shell conditions are:

$$\begin{aligned} a_5 &= \alpha_1(\beta_1 + \beta_{k_1})s - q_{1t}^2 = 0 \\ a_9 &= (\alpha - \alpha_1)(-\beta_1)s - q_{t1}^2 = 0. \end{aligned} \tag{29}$$

There are two different sets of solutions for small values of q_{t1}^2/s. The first set corresponds to α_1 and $\beta_1 = \mathcal{O}(q_{t1}^2/s)$, while the second set corresponds to $\alpha - \alpha_1$ and $\beta_{k_1} + \beta_1 = \mathcal{O}(q_{t1}^2/s)$. This last case contributes only at the subleading level. The case of interest is the first one:

$$\alpha_1 \simeq \frac{q_{t1}^2}{\beta_{k_1} s}, \qquad \beta_1 \simeq \frac{-q_{t1}^2}{\alpha s}.$$

The denominators corresponding to the parton lines of interest are:

$$\begin{aligned}
a_1 \qquad & (q_2 - Q)^2 = \alpha_2(\beta_2 - \beta_Q)s - q_{t2}^2 + i\epsilon \\
a_2 \qquad & (k_2 + q_2)^2 = \alpha_2(\beta_2 + \beta_{k_2})s - q_{t2}^2 + i\epsilon \\
a_3 \qquad & (q_2)^2 = \alpha_2\beta_2 s - q_{t2}^2 + i\epsilon \\
a_2' \qquad & (k_2 + Q - q_2)^2 = -\alpha_2(\beta_{k_2} + \beta_Q - \beta_2)s - q_{t2}^2 + i\epsilon \\
a_4 \qquad & (q_1 + Q)^2 \simeq \frac{\beta_Q - \beta_{k_1}}{\beta_{k_1}} q_{t1}^2 \\
a_6 \qquad & (q_1)^2 \simeq -q_{t1}^2 \\
a_7 \qquad & (p - q_2 + Q)^2 = (\alpha - \alpha_2)(-\beta_2 + \beta_Q)s - q_{t2}^2 + i\epsilon \\
a_7' \qquad & (p - q_1 - Q)^2 = (\alpha - \alpha_1)(-\beta_Q)s + i\epsilon \\
a_8 \qquad & (p - q_1 - q_2)^2 = (\alpha - \alpha_1)(-\beta_2)s + \alpha_2(\beta_1 + \beta_2)s + q_{t1}^2 - q_t^2 + i\epsilon \\
a_8' \qquad & (p + Q)^2 = \alpha\beta_Q s + i\epsilon.
\end{aligned}$$

The variables to be integrated are β_2, α_2 and β_Q. The limits of integration of β_Q, namely $-\beta_{k_2}$ and β_{k_1}, are not affected by the constraints imposed by the cuts. The limits for α_2 are a consequence of the integration on β_2, to obtain a result different from zero one needs to have $0 \leq \alpha_2 \leq \alpha$. The leading contribution comes from the region $\alpha_2 = \mathcal{O}(q_t^2/s)$. One observes that the transverse momenta q_{ti} can be neglected, in this case, in a_7, a_7' and a_8: if one introduces the positions of the poles of $1/a_7$, $1/a_7'$ and $1/a_8$ in the other lines, terms of kind $\beta_i \approx q_t^2/s$ multiplied by $\alpha_i s$ are introduced. The term $\alpha_i q_t^2$ that is generated is much smaller

with respect to the term q_t^2 already present. On the contrary, if the positions of the poles of the vertical lines are introduced in the horizontal ones, terms of kind $q_t^2/(\alpha_i s) \gg q_t^2$ are generated so that the original q_t can be neglected. Finally if the positions of the singularities of $1/a_7$, $1/a_7'$ and $1/a_8$ are introduced in $1/a_7$, $1/a_7'$ and $1/a_8$ no critical dependence is generated in the $q_t^2/s \to 0$ limit. Keeping only terms where the integration variables are multiplied by s, a_7, a_7' and a_8 are expressed as:

$$\begin{aligned} a_7 \qquad & (p-q_2+Q)^2 = \alpha(-\beta_2+\beta_Q)s + i\epsilon \\ a_7' \qquad & (p-q_1-Q)^2 = -\alpha\beta_Q s + i\epsilon \\ a_8 \qquad & (p-q_1-q_2)^2 = -\alpha\beta_2 s + i\epsilon \end{aligned}$$

The graphs of fig.12 correspond to the following integral:

$$\int \frac{1}{a_1 a_3 a_4 a_6}\Big(\frac{1}{a_2}+\frac{1}{a_2'}\Big)\Big(\frac{1}{a_7 a_8}+\frac{1}{a_7 a_8'}+\frac{1}{a_7' a_8}\Big)\delta(a_9)\delta(a_5). \tag{30}$$

Having neglected the q_t terms in a_7, a_7' and a_8, one can write:

$$\begin{aligned} &\Big(\frac{1}{a_7 a_8}+\frac{1}{a_7 a_8'}+\frac{1}{a_7' a_8}\Big) \\ &\qquad = \frac{1}{\alpha\beta_2 s - i\epsilon}\Big(\frac{1}{\alpha\beta_Q s - i\epsilon} - \frac{1}{\alpha\beta_Q s + i\epsilon}\Big) \end{aligned}$$

in such a way that the integral on β_2 can be done taking the residuum of the pole $(\alpha\beta_2 s - i\epsilon)^{-1}$ and Eq.(30) is expressed as:

$$\begin{aligned} \int_0 \frac{d\alpha_2 d\beta_Q}{-\alpha_2\beta_Q s - q_{t2}^2 + i\epsilon}\frac{1}{q_{t2}^2}\Big(\frac{1}{\alpha_2\beta_{k_2}s - q_{t2}^2 + i\epsilon} + \frac{1}{-\alpha_2(\beta_{k_2}+\beta_Q)s - q_{t2}^2 + i\epsilon}\Big) \\ \times \Big(\frac{1}{\alpha\beta_Q s - i\epsilon} - \frac{1}{\alpha\beta_Q s + i\epsilon}\Big)\frac{\beta_{k_1}}{\beta_Q - \beta_{k_1}}\frac{(2\pi)^3}{\alpha^2\beta_{k_1}s^3(q_{t1}^2)^2}. \end{aligned} \tag{31}$$

The integral on β_Q is done taking the residuum of the pole $(\alpha\beta_Q s - i\epsilon)^{-1}$:

$$\int d\beta_Q\Big(\frac{1}{\alpha\beta_Q s - i\epsilon} - \frac{1}{\alpha\beta_Q s + i\epsilon}\Big) = \oint \frac{d\beta_Q}{\alpha\beta_Q s - i\epsilon}$$

The integral on α_2 receives its major contribution from the imaginary part of $1/a_2'$, since the singularity of $1/a_2$ is outside the integration domain. The resulting

leading term, after keeping into account the multiplicity factor mentioned in the beginning of the paragraph, is:

$$\frac{4\pi(2\pi)^4}{\beta_{k_1}\beta_{k_2}\alpha^3 s^5}\frac{1}{(q_{t1}^2)^2(q_{t2}^2)^2} \tag{32}$$

that is twice the leading contribution obtained when discussing the two box cut case.

Case b

The second possibility is that one of cutting a vertical and a horizontal line. The set of cut diagrams that we consider is shown in fig.13. The mass shell conditions are:

$$\begin{aligned} a_4 &= \alpha_1(\beta_1+\beta_Q)s - q_{1t}^2 = 0 \\ a_9 &= (\alpha-\alpha_1)(-\beta_1)s - q_{t1}^2 = 0. \end{aligned} \tag{33}$$

The reality of the solutions imply for β_Q:

$$\frac{4q_{t1}^2}{\alpha s} \leq \beta_Q \leq \beta_{k_1}$$

and, in the $q_t^2/s \to 0$ limit, the solution of interest of Eq.(33) is:

$$\alpha_1 \simeq \frac{q_{t1}^2}{\beta_Q s}, \qquad \beta_1 \simeq \frac{-q_{t1}^2}{\alpha s}$$

with $\beta_Q \neq \mathcal{O}(q_t^2/s)$. The denominators corresponding to the parton lines of interest are:

a_1 $\quad (q_2-Q)^2 = \alpha_2(\beta_2-\beta_Q)s - q_{t2}^2 + i\epsilon$

a_2 $\quad (k_2+q_2)^2 = \alpha_2(\beta_2+\beta_{k_2})s - q_{t2}^2 + i\epsilon$

a_3 $\quad (q_2)^2 = \alpha_2\beta_2 s - q_{t2}^2 + i\epsilon$

a_2' $\quad (k_2+Q-q_2)^2 = -\alpha_2(\beta_{k_2}+\beta_Q-\beta_2)s - q_{t2}^2 + i\epsilon$

a_5 $\quad (k_1+q_1)^2 \simeq \frac{\beta_{k_1}-\beta_Q}{\beta_Q}q_{t1}^2$

a_5' $\quad (k_1-Q-q_1)^2 \simeq \frac{-\beta_{k_1}}{\beta_Q}q_{t1}^2$

$$
\begin{aligned}
a_6 \qquad & (q_1)^2 \simeq -q_{t1}^2 \\
a_7 \qquad & (p - q_2 + Q)^2 = (\alpha - \alpha_2)(-\beta_2 + \beta_Q)s - q_{t2}^2 + i\epsilon \\
a_7' \qquad & (p - q_1 - Q)^2 = -\alpha\beta_Q s + q_{t1}^2 \\
a_8 \qquad & (p - q_1 - q_2)^2 = -(\alpha - \alpha_1 - \alpha_2)\beta_2 s + \alpha_2\beta_1 s + q_{t1}^2 - q_t^2 + i\epsilon \\
a_8' \qquad & (p + Q)^2 = \alpha\beta_Q s.
\end{aligned}
$$

Analogously to the a *case* one can neglect the transverse momenta in a_7, a_7' and a_8. The diagrams in fig.13 correspond to the integral

$$
\int \frac{1}{a_1 a_3 a_6}\Big(\frac{1}{a_2} + \frac{1}{a_2'}\Big)\Big(\frac{1}{a_7 a_8} + \frac{1}{a_7 a_8'} + \frac{1}{a_7' a_8}\Big)\Big(\frac{1}{a_5} + \frac{1}{a_5'}\Big)\delta(a_9)\delta(a_4) \qquad (34)
$$

The main difference from the previous case comes from the domain of integration on β_Q: while in *case* a β_Q was both positive and negative and values of β_Q of order q_t^2/s where allowed, in the present case the conditions of reality for the cut parton lines force β_Q to take positive values only and the requirement $\alpha_1 = \mathcal{O}(q_t^2/s)$ excludes the domain $\beta_Q = \mathcal{O}(q_t^2/s)$. As a consequence, while previously

$$
\int \Big(\frac{1}{a_7 a_8} + \frac{1}{a_7 a_8'} + \frac{1}{a_7' a_8}\Big) d\beta_2 d\beta_Q = \mathcal{O}\Big(\frac{1}{s^2}\Big),
$$

it is presently contributing with a factor of order q_t^2/s^3 only. As a consequence the contributions from cuts of this kind are suppressed by a factor q_t^2/s with respect to the leading.

III.3 No cut boxes

The last case to be considered is that one where the target parton lines are not cut. The graphs to be considered in this case are shown in fig.14. The mass shell condition is:

$$
a_8' = (p + Q)^2 = \alpha\beta_Q s = 0
$$

that implies $\beta_Q = 0$. The denominators to be integrated can be written as:

$$
\begin{aligned}
a_1 \qquad & (q_2 - Q)^2 = \alpha_2\beta_2 s - q_{t2}^2 + i\epsilon \\
a_2 \qquad & (k_2 + q_2)^2 = \alpha_2(\beta_2 + \beta_{k_2})s - q_{t2}^2 + i\epsilon \\
a_3 \qquad & (q_2)^2 = \alpha_2\beta_2 s - q_{t2}^2 + i\epsilon \\
a_2' \qquad & (k_2 + Q - q_2)^2 = -\alpha_2(\beta_{k_2} - \beta_2)s - q_{t2}^2 + i\epsilon \\
a_4 \qquad & (q_1 + Q)^2 = \alpha_1\beta_1 s - q_{t1}^2 + i\epsilon \\
a_5 \qquad & (k_1 + q_1)^2 = \alpha_1(\beta_1 + \beta_{k_1})s - q_{t1}^2 + i\epsilon \\
a_6 \qquad & (q_1)^2 = \alpha_1\beta_1 s - q_{t1}^2 + i\epsilon \\
a_5' \qquad & (k_1 - Q - q_1)^2 = \alpha_1(\beta_1 - \beta_{k_1})s - q_{t1}^2 + i\epsilon \\
a_7 \qquad & (p - q_2 + Q)^2 = (\alpha - \alpha_2)(-\beta_2)s - q_{t2}^2 + i\epsilon \\
a_9 \qquad & (p - q_1)^2 = (\alpha - \alpha_1)(-\beta_1)s - q_{t1}^2 + i\epsilon \\
a_7' \qquad & (p - q_1 - Q)^2 = (\alpha - \alpha_1)(-\beta_1)s - q_{t1}^2 + i\epsilon \\
a_9' \qquad & (p - q_2)^2 = (\alpha - \alpha_2)(-\beta_2)s - q_{t2}^2 + i\epsilon.
\end{aligned}
$$

The first four graphs in fig.14, that have to be integrated on α_1, β_1, α_2 and β_2, are represented by the expression:

$$\int \frac{1}{a_1 a_3}\Big(\frac{1}{a_2} + \frac{1}{a_2'}\Big)\frac{1}{a_7 a_4 a_6}\Big(\frac{1}{a_5} + \frac{1}{a_5'}\Big)\frac{1}{a_9}\delta(a_8') \tag{35}$$

while the graphs in the second line in fig.14 correspond to:

$$\int \frac{1}{a_1 a_3}\Big(\frac{1}{a_2} + \frac{1}{a_2'}\Big)\frac{1}{a_9' a_4 a_6}\Big(\frac{1}{a_5} + \frac{1}{a_5'}\Big)\frac{1}{a_7'}\delta(a_8''). \tag{36}$$

The two contributions are explicitly equal. Let us compute the first one. The integrations on α_2, β_2 involve a_1, a_3 a_2, a_2' and a_7. The β_2 integration is evaluated taking the residuum of the pole $1/a_7$ that gives for β_2 the value

$$\beta_2 = \frac{-q_{t2}^2}{(\alpha - \alpha_2)s}$$

while the α_2 integration is restricted to the interval:

$$0 \leq \alpha_2 \leq \alpha$$

The dominant contribution comes from the region $\alpha_2 \to 0$:

$$\int \frac{1}{a_1 a_3}\Big(\frac{1}{a_2}+\frac{1}{a_2'}\Big)\frac{1}{a_7} \approx \int_0 \frac{2\pi d\alpha_2}{\alpha s (q_{t2}^2)^2}\Big(\frac{1}{\alpha_2\beta_{k_2}s - q_{t2}^2 + i\epsilon}+\frac{1}{-\alpha_2\beta_{k_2}s - q_{t2}^2 + i\epsilon}\Big). \tag{37}$$

In the limit $q_t^2/s \to 0$ the leading term to the integral is provided by the imaginary part of $1/a_2$.

The integrations on α_1, β_1 involve a_4, a_6, a_5, a_5' and a_9. The integral on β_1 is done taking the residuum of $1/a_9$ while that on α_1 is performed analogously to the α_2 integration. The contribution from the *no cut boxes* case, resulting from the sum of the graphs in fig.14, is expressed as:

$$\frac{1}{\alpha^3\beta_{k_1}\beta_{k_2}s^5}\frac{\pi(2\pi)^4}{q_{t1}^2 q_{t2}^2} \tag{38}$$

that is half of the contribution obtained in the *two box cut* case and 1/4 of the contribution obtained in the *one box cut* case.

One can then conclude that the leading contributions to the cut semi-hard rescattering diagrams are proportional to one another and the weight factors are precisely the A.G.K. weights[9]. Even more, the leading contribution comes from the configuration where the intermediate projectile parton, between the two successive semi-hard collisions, is on shell. As a consequence the three body cross section is factorized as the product of two body interaction probabilities.

IV. Discussion and conclusions

The set of Feynman diagrams in fig.2 is the complete set of diagrams contributing, at the lowest order g^8, to the isospin component of the three body amplitude characterized by the base-isospin diagram in fig.3. The leading behavior of each of the diagrams in fig.2 and of all the different cuts of the amplitude, dominant in the high s fixed t limit, have been explicitly evaluated in the previous paragraphs. Each of the different cuts of the amplitude is obtained by summing a different sub-set of cut diagrams. The leading behavior of every different cut amplitude grows less rapidly with s than each single cut diagram in the corresponding sum. The relevant contribution of each single diagram to the cut amplitude is therefore a subleading one. The efficient way, which we have adopted to account

for all interferences between the different terms, has been to evaluate directly the leading behavior of the sum, rather than working out, in advance, all subleading terms of every single different diagram. In this last paragraph we like to remark a few interesting properties of the amplitude under consideration and we describe the physical picture of the interaction which results.

Semi-hard interactions are connected with the presence of different scales. In fact, in our case, there are three different scales: the nucleon-nucleon c.m. energy $\sqrt{s}$, the cut off q_t^{min}, and the typical hadronic scale which we have called m. Moreover the relation $\sqrt{s} \gg q_t^{min} \gg m$ holds. When studying parton interactions, without keeping into account that partons are bound in the hadron, one is assuming that, at least to work out the leading terms, one is allowed to split the semi-hard part of the interaction from the binding effects. Namely one assumes to be allowed to neglect, at that stage of the calculation, the virtuality and transverse momenta of projectile and target partons. A consistency requirement is therefore that the scale of the virtuality and of the transverse momenta of the partons in the loop integrals is provided by q_t^{min}, while the analogous scale for the incoming and outgoing projectile and target partons is rather m. This consistency requirement is met when the integrations on the longitudinal variables α_1, α_2, β_1, β_2 and β_Q are all done within the kinematical configurations relevant for the eikonal. More explicitly, the behavior of the integrand at infinity has to be regular enough, in such a way that, in all cases, the contours may be closed without need of specifying the position of further singularities other than the ones in the eikonal region. When the contour cannot be closed, the kinematics of the interaction is not constrained enough and configurations, far from the eikonal ones, became important as well. To perform the integral on β_Q, which is a variable external to the loop integrals, one should consider, in that case, the singularities of the non-perturbative part too.

The set of diagrams in fig.2 allows one to meet this consistency requirement. In fact the behavior of the integrand, far from the singular points of the propagators in the set of diagrams of fig.2, is always convergent rapidly enough, in such a way that the contour can always be closed at infinity. One notices that this is a property of the sum of all the space-time parts of the diagrams in fig.2, when dealing with the uncut amplitude, and of the sum of all cut diagrams contributing to the same final state, when looking to the cut amplitude. It is not a property of each single diagram or cut diagram. In the sum of diagrams in fig.2 one finds, in fact, that,

when a term does not converge sufficiently well at infinity, there is always another one, in the $q_t^2/s \to 0$ limit, with the same behavior but with opposite sign. One may notice that, when logs appear, the convergence at infinity is not fast enough. In that case the corresponding integration variable is not restricted to a particular range and all possible values contribute to the final result. Consistently with this observation, both the G_1 component of the amplitude $M_{III} + M_{II}$, considered in the first part of the paper, and the corresponding cuts of the amplitude, which have been discussed in the second part, do not contain any ln$s$.

Some of the different cuts of the same diagram are related. In the set of diagrams in fig.13, one could select a few terms in the central column and compare with the corresponding terms in fig.14. The contributions are related as a consequence of the suppression of the amplitude corresponding to each one of the first eight uncut diagrams in fig.2, which has been discussed in subsection a of paragraph **II**. Rather than putting in evidence this compensation between different cuts of the same diagram[8], we add separately all cut diagrams in fig.13 and in fig.14 because we want to keep into account all interferences of the different contributions to the same final state. Differently with respect of the cut diagrams in fig.14, the resulting contribution, from the whole sum of cut diagrams in fig.13, is a subleading one. Specifically, consider the first diagram in fig.2, the corresponding contribution to the cut shown in fig.13 (second cut-diagram in the first line of fig.13) is compensated by one of the contributions from the first cut-diagram in the same line. In detail, with reference to Eq.(34), where the term corresponding to the first diagram in the first line of fig.13 is $1/a_7 a_8$, one obtains two contributions from the integration on β_2, one from the pole $1/a_7$, the second from $1/a_8$. The first of the two contributions is the one which interferes destructively: For $a_7 = 0$, $a_8 = -\alpha\beta_Q s + \mathcal{O}(q_t^2) + i\epsilon$. The second diagram in fig.13 is obtained from this term by the replacement $1/a_8 \to 1/a_8'$, where $a_8' = \alpha\beta_Q s + i\epsilon$. The sum of the two terms contains the factor $(1/a_8 + 1/a_8') = \mathcal{O}\big(1/s \times (q_t^2/s)\big)$, because the cut in fig.13 does not allow the two propagators, $1/a_8$ and $1/a_8'$, to go on shell. As discussed in section **III.2**, *case* **a**, the compensation just mentioned does not occur when the cut allows the configuration with the intermediate propagators $1/a_8$ and $1/a_8'$ on shell, as in the case of the cut diagrams in fig.12. In fact, while the real parts of $1/a_8$ and $1/a_8'$ are canceled in the sum, the imaginary parts are, on the contrary, added.

In ref.8 double ladder exchanges are discussed in QCD, limiting the analysis to the diagrams with the leading behavior at high energy. We have studied the simplest case of the double box exchange in a three body interaction. In our framework, which is consistent with the Reggeized gluon framework, we have taken into account of all the diagrams which contribute, at the lowest order in g, to the color factor shown in fig.3, which is also the color factor selected by using the criterion of the leading behavior of ref.8. The set of diagrams, which we have taken into account, is gauge independent and contains both leading (set III) and non-leading (set II and set I) diagrams at high energy. As a consequence of destructive interferences between different terms, contributions subleading at large s acquire the same importance as the leading ones in our analysis. Actually the diagrams of set II, which are of order $\ln s$, contribute to the final result to the same extent as the diagrams in set III, which are of order $(\ln s)^2$.
The physical picture which we obtain is considerably different from the one obtained by selecting the leading diagrams only. After grouping all cut diagrams, which contribute to the same final state, and considering the leading contributions, for $(q_t^{min})^2/s \to 0$, only a restricted number of cut diagrams contribute at the leading order. These are the cut diagrams shown in fig.9, in fig.12 and in fig.14. The leading terms, corresponding to the different kinds of cuts, are all proportional to one another with given weight factors, that are equal to the A.G.K. weights[9]. The same destructive interference, which cancels the dominant real parts of the different cut diagrams, is the mechanism which selects, as a dominant contribution to the loop integration, the imaginary part of the intermediate propagators of the projectile and target partons. The leading configuration, where the projectile parton is on shell between successive interactions, allows, correspondingly, the probabilistic physical picture where the three body interaction is factorized as the product of two successive collisions between pairs of on shell partons. One may notice that the intermediate propagator, as expected from an analysis of the rescattering diagram by means of the Landau equations[15], contributes with a factor of order $1/s$ to the loop integral. In the case of the pinch singularity, obtained by summing two different propagators with opposite real parts, the values for the virtuality of the intermediate propagator, while performing the loop integral, are of order q_t^2. The integration range of the relevant integration variable is however of order q_t^2/s, in such a way that an overall factor of $1/s$ is obtained.

In all the leading cut amplitudes, considered here, only the projectile and target parton lines are cut. Accordingly, the main contribution to the inelastic cross section is localized in the projectile and target fragmentation regions. Already in an Abelian theory one can find graphs with more particles in the s-channel, which contribute rather to the production in the central region. Moreover, in the three body scattering, graphs, which are not trivially related to the ones present in the two body scattering, arise. An example is got if we read term 4 in fig.7 as a standard Feynman graph: it cannot enter in the process of gluon Reggeization, it could better, if the Reggeization program works completely, begin to build up a three-Reggeon vertex. The feature, which characterizes the term of the three body amplitude studied here, is that it is related to the part of the inelastic cross section where all partons scatter without production.

Acknowledgment

Useful and stimulating discussions with P.V. Landshoff are gratefully acknowledged.

Appendix A

In this appendix we wish to discuss some problems connected with the gauge and spin properties of the particles involved in the processes discussed in the paper which, according to the standard point of view, are described as massless quarks and massless gluons.
It is well known that in order to connect parton model with perturbative QCD it is better to use a gauge where there is no need of ghosts and one of the most usually employed is the axial gauge[16]. The relevant kinematical variables of the problem suggest for the gauge vector c_μ the choice $c_\mu \equiv (1;\mathbf{0})$, so we make the choice which is sometimes referred as temporal gauge[17]. The general form of the gluon propagator:

$$\Delta_{\mu\nu}(l) = \frac{1}{l^2}\left\{g_{\mu\nu} - \frac{c_\mu l_\nu + c_\nu l_\mu}{c\cdot l} + c^2\frac{l_\mu l_\nu}{(c\cdot l)^2}\right\}$$

is then reduced to:

$$\Delta_{00} = 0, \qquad \Delta_{0j} = 0 \qquad \Delta_{ij} = \frac{1}{l^2}\left\{-\delta_{ij} + \frac{l_i l_j}{l_0^2}\right\} \tag{A1}$$

When we take into account the lines carrying momenta p or k we assume consistently with all the treatment that $q \ll p_0$ or k_0 so that the most important term in the numerator is:

$$-\delta_{ij} + \frac{p_i p_j}{p_0^2}$$

and since $p_z = p_0$, the propagator, in this case reduces to:

$$\Delta_{ab} = -\frac{1}{(p+q)^2}\delta_{ab} \qquad a,b = 1,2 \qquad\qquad \Delta_{a3} = \Delta_{33} = \mathcal{O}(q/p_0) \tag{A2}$$

Now one inserts between two propagators the vertex $J_{\lambda\mu\nu}$ (fig15a):

$$J_{\lambda\mu\nu} = (2p+q)_\mu g_{\lambda\nu} + (-p-2q)_\lambda g_{\mu\nu} + (q-p)_\nu g_{\mu\lambda} \tag{A3}$$

It is evident that the first addendum alone builds up the leading term because the large, longitudinal parts of the second and third addendum are eliminated by contracting the expression of Eq.($A3$) with the ones of Eq.($A2$). The conclusion in that the leading term corresponding to the horizontal line of fig.15a is:

$$\delta_{ab}\frac{(2p+q_1)_{\mu_1}}{(p+q_1)^2}\cdot\frac{(2p+q_1+q_2)_{\mu_2}}{(p+q_1+q_2)^2}\cdots\frac{(2p+\sum q)_{\mu_n}}{(p+\sum q)^2} \tag{A4}$$

while if one of the indices of the line carrying momentum p is either 3 or 0 we get only a subleading contribution and the terms in q are there only as a remnant of many subleading terms. If we consider the lines carrying the momenta k the result is the same. Now we proceed to connecting the subgraphs in order to obtain the general form like fig.15b. For the vertical line the form of the propagator is given by Eq.($A1$) and, if we come back to the light cone variables, we find that the factor of the general expression corresponding to two vertices and a vertical propagator takes, in its leading term, the form:

$$\frac{s}{q^2}\alpha_p\beta_k\frac{4\alpha_q\beta_q}{(\alpha_q+\beta_q)^2}. \tag{A5}$$

This expression, by suitable iteration gives finally rise to the whole expression of the leading terms in s of the amplitude represented by fig15*b*. which has the properties we used in the discussions of this paper, in particular in the individuation of the most important terms in the cut graphs.
If the horizontal lines are fermionic the problem is simpler, it is known from standard QED that for large energy and small momentum transfer the convective part of the current is the most important. A simple exercise on $\gamma-$matrices reproduces the result:

$$\frac{\hat{p}+\hat{q}}{(p+q)^2}\gamma_\mu\frac{\hat{p}+\hat{q}+\hat{q'}}{(p+q+q')^2}$$
$$=2(p+q)_\mu\frac{1}{(p+q)^2}\cdot\frac{\hat{p}+\hat{q}+\hat{q'}}{(p+q+q')^2}-\gamma_\mu\frac{\hat{p}+\hat{q}}{(p+q)^2}\frac{\hat{p}+\hat{q}+\hat{q'}}{(p+q+q')^2}$$

In the second addendum, using the fact that $p^2=0$, we get a factor of p less than in the first one, which gives just the convective part of the current; the procedure can be iterated and we end up with an expression like Eq.($A4$). Since there is no way in which the terms till now considered might disappear it is correct to classify all the neglected terms as subleading ones. The case, finally, where there is a quark in the vertical line corresponds in our kinematical frame to a backward scattering of a gluon by a quark and is therefore suppressed. This result, obtained in axial gauge, can be translated in Feynman gauge. It is well known that there is no straightforward correspondence between the graphs drawn starting from the two gauges. Nevertheless it holds for the graphs which we have chosen, because there are no graphs containing ghosts at that perturbative order and with the prescribed quantum number exchange between the projectile and the targets.

Appendix B

The aim of this appendix is to review with some more detail the high s behavior of the uncut graphs,with particular attention to the role of some subleading terms.As already seen the 24 graphs of "eikonal type",i.e. graphs where neither gluon branching nor four-gluon interaction are present can be easily grouped into three families which can be called the two-boxes,box in the box and pentagonal graphs and correspond respectively to graphs 1–8,17–24,9–17 of fig.2 (see also

fig.5). Since there is an obvious symmetry between the two target quarks it is enough to study 12 graphs,four in each of the three families. As in all the previous discussions the integration will be performed over the longitudinal variables at fixed transverse ones;since we integrate also over the longitudinal variable which represents the difference between the "minus" component of the target momenta we have,in the whole,a five-fold integral.

two-box graphs

For this family nothing relevant has to be added to what was already said, in fact even if we keep in the expression those transverse variable that were discarded in the previous discussion it is still possible to bring the integrand in β_Q in a form having all its poles on the same side of the real axis and decreasing fast enough to the infinity so that the overall result is zero.

box in the box

One of the possible integrands,the one corresponding to the term 17 in fig.2 is

$$\begin{aligned} I_{17} =& \frac{1}{\alpha_2(\beta_{k_2}+\beta_2)s-q_{2t}^2}\frac{1}{\alpha_1(\beta_{k_1}+\beta_1)s-q_{1t}^2} \\ &\times\frac{1}{\alpha_2(\beta_2-\beta_Q)s-q_{2t}^2}\frac{1}{\alpha_2\beta_2 s-q_{2t}^2}\frac{1}{\alpha_1(\beta_1+\beta_Q)s-q_{1t}^2}\frac{1}{\alpha_1\beta_1 s-q_{1t}^2} \\ &\times\frac{1}{(\alpha-\alpha_2)(\beta_Q-\beta_2)s-q_{2t}^2}\frac{1}{(\alpha-\alpha_2)\beta_2 s+q_{2t}^2}\frac{1}{(\alpha-\alpha_1-\alpha_2)(\beta_1+\beta_2)s+q_t^2} \end{aligned} \tag{B.1}$$

whereas the other three terms 18,19,20 in the same fig.2 show analogous forms which are not reported here. The integration over the variables β_1,β_2,β_Q leads to the expressions

$$\begin{aligned} I_{17} =& \frac{i(2\pi)^3\alpha_2^2}{(\alpha-\alpha_1-\alpha_2)s^4\beta_{k_2}}\left(\frac{1}{\alpha_1\alpha_2\beta_{k_1}s-\mathcal{A}}\frac{1}{\mathcal{A}^2}\frac{1}{q_{2t}^4}\right. \\ &\left.-\frac{1}{\alpha_1\alpha_2(\beta_{k_1}+\beta_{k_2})s-\mathcal{A}}\frac{1}{\mathcal{A}}\frac{1}{q_{2t}^2}\frac{1}{\alpha_1\alpha_2\beta_{k_2}s-\mathcal{A}}\frac{1}{\alpha_2(1-\alpha_2)\beta_{k_2}s+q_{2t}^2}\right), \end{aligned} \tag{B.2}$$

where the following notations have been used:

$$\begin{aligned} \mathcal{A} =& \alpha_1 q_{2t}^2+\alpha_2 q_{1t}^2+\alpha_0 q_t^2 \\ \alpha_0 =& \frac{\alpha_1\alpha_2}{\alpha+\alpha_1+\alpha_2}. \end{aligned} \tag{B.3}$$

It is useful to note that all the four expressions consist,as the one explicitly displayed, of two addenda showing this common feature:the first one gives a larger contribution for $s \to \infty$ because it has fewer s in the denominators,the second one gives a relevant contribution only when the α-parameters are very small,so that they can cancel the effect of the s in the denominators;the origin of this difference may be traced back to the integration over the β variables,where it is unavoidable, at a certain step,to take into account at least two poles;one of which has its position depending on the external variables β_{k_1}, β_{k_2},which are of the order 1. We are interested in keeping the cutoff on the transverse momenta,since this justifies the use of the perturbative expansion,but the sign of the transverse variables is irrelevant,so $\mathbf{q_i}$ is wholly equivalent to $-\mathbf{q_i}$.

We realize that the "large terms" in eq. B.3 cancel in pairs whilst the subleading term of the four expressions are in general different so that they do not cancel. If we study the large s behavior of the single large term of eq. B.2 we find that it behaves as $s^{-5}(\ln s)^2$,moreover when the overall phase makes this leading term real there is an imaginary part going as $s^{-5}(\ln s)$. The "small terms" give in general contributions going as s^{-5},so this is the behavior of the sum.

pentagons

One of the possible integrands,corresponding to the term 9 in fig.2 is

$$\begin{aligned} I_9 =& \frac{1}{\alpha_2(\beta_{k_2}+\beta_2)s - q_{2t}^2} \frac{1}{\alpha_1(\beta_{k_1}+\beta_1)s - q_{1t}^2} \\ &\times \frac{1}{\alpha_2(\beta_2-\beta_Q)s - q_{2t}^2} \frac{1}{\alpha_2\beta_2 s - q_{2t}^2} \frac{1}{\alpha_1(\beta_1+\beta_Q)s - q_{1t}^2} \frac{1}{\alpha_1\beta_1 s - q_{1t}^2} \\ &\times \frac{1}{(\alpha-\alpha_2)(\beta_Q-\beta_2)s - q_{2t}^2} \frac{1}{(\alpha-\alpha_2)\beta_1 s + q_{1t}^2} \frac{1}{(\alpha-\alpha_1-\alpha_2)(\beta_1+\beta_2)s + q_t^2} \end{aligned} \tag{B.4}$$

with other three analogous expressions for the terms 10,11,12. We perform the integrations over the three variables β and we find here also larger and smaller contribution due to the necessity of taking the contributions of two poles. We could use only the larger contributions, arising from terms $I_9, I_{10}, I_{11}, I_{12}$ producing in this way the expression:

$$I_\pi = \frac{i(2\pi)^3}{(\alpha-\alpha_1-\alpha_2)s^5\beta_{k_2}\beta_{k_1}} \frac{1}{\alpha_1\alpha_2\beta_{k_2}s - \mathcal{A}} \frac{1}{\alpha_1\alpha_2\beta_{k_1}s + \mathcal{A}} \frac{1}{q_{2t}^2} \frac{1}{q_{1t}^2} \tag{B.5}$$

were it not for an end point singularity which is produced in this way,but which is wholly artificial;if we consider also the small contribution,at least for the relevant integral ,i.e.

$$I_{\varpi} = \frac{i(2\pi)^3}{(\alpha-\alpha_1-\alpha_2)s^5\beta_{k_2}\beta_{k_1}} \frac{1}{-\alpha_1(\alpha-\alpha_1)\beta_{k_1}s} \frac{1}{\alpha_1\alpha_2\beta_{k_1}s+\mathcal{A}} \frac{1}{q_{2t}^2} \frac{1}{\mathcal{A}} \qquad (B.6)$$

we find,in fact,by studying in detail the behavior of the expression at the end points of the integration domain that the singularity is no longer present. The actual evaluation implies the separation of the principal part and of the pole contribution,both of them give contributions going as s^{-5},whilst in single terms of B.5 we can find behaviors like $s^{-5}\ln s$.

This analysis confirms that the logarithmic behavior in the total energy is present in the single terms,even the squared logarithm growth,in the graphs of the family "box in the box" but summing the terms family by family only the power behavior survives.

References

1) H. Cheng and T.T. Wu, *Phys. Rev.* **186** (1969) 1611.

2) B.M. McCoy and T.T. Wu, *Phys. Rev. Lett.* **35** (1975) 604, *Phys. Rev.* **D13** (1976) 1076; V.S. Fadin, E.A. Kuraev and L.N. Lipatov, *Phys. Lett.* **B60** (1975) 50; L.Łukaszuk and X.Y. Pham, *Phys. Lett.* **B53** (1974) 287; H.T. Nieh and Y.P. Yao, *Phys. Rev.* **D13** (1976) 1082; L. Tyburski, *Phys. Rev.* **D13** (1976) 1107; L.L. Frankfurt and V.E. Sherman, *Sov. J. Nucl. Phys.* **23** (1976) 581; C.Y. Lo and H. Cheng, *Phys. Rev.* **D13** (1976) 1131; P.S. Yeung, *Phys. Rev.* **D13** (1976) 2306; H. Cheng and C.Y. Lo, *Phys. Rev.* **D15** (1977) 2959.

3) H. Cheng, J.A. Dickinson and K. Olaussen, *Phys. Rev.* **D23** (1981) 534.

4) H. Cheng and T.T. Wu, *Expanding Protons: Scattering at High Energies*, The MIT Press 1987.

5) P.S. Yeung, *Phys. Rev.* **D23** (1981) 1003.

6) M.T. Grisaru, H.J. Schnitzer and H.S. Tsao *Phys. Rev. Lett* **30** (1973) 811.

7) M.G. Ryskin and Yu.M. Shabelski, *Z. Phys.* **C56** (1992) 253.

8) L.V. Gribov, E.M. Levin and M.G. Ryskin, *Phys. Reports* **100** (1983) 1.

9) V.A. Abramovskii, V.N. Gribov and O.V. Kancheli, *Yad. Fiz.* **18** (1973) 595, (*Sov. J. Nucl. Phys.* **18** (1974) 308).

10) C.Y. Lo, *Phys. Rev.* **D23** (1981) 508.

11) W.R. Chen and R.C. Hwa, *Phys. Rev.* **D39** (1989) 179; T.K. Gaisser and T. Stanev, *Phys. Lett.* **B219** (1989) 375; L. Durand and H. Pi, *Phys. Rev.* **D40** (1989) 1436; M.M. Block, R.S. Fletcher, F. Halzen B. Margolis and P. Valin, *Phys. Rev.* **D41** (1990) 978; P. Aurenche, F.W. Bopp, A. Capella, J. Kwiecinski, M. Maire, J. Ranft and J. Tran Thanh Van *Phys. Rev.* **D45** (1992) 92;

12) G. Calucci and D. Treleani, *Phys. Rev.* **D41** (1990) 3367; **D44** (1991) 2746.

13) R.J. Eden, P.V. Landshoff, D.I. Olive and J.C. Polkinghorne, *The Analytic S-Matrix*, Cambridge University Press 1966.

14) D. Amati, S. Fubini and A. Stanghellini, *Nuovo Cimento* **26** (1962) 896.

15) L.D. Landau, *Proceedings of the Kiev Conference on High Energy Physics* (1959) (unpublished); *Nucl. Phys.* **13** (1959) 181; J.D. Bjorken (1959). Stanford University Ph.D. thesis; J. Mathews, *Phys. Rev.* **113** (1959) 381; N. Nakanishi *Prog. Theor. Phys.* **21** (1959) 135.

16) I.B. Khriplovich, *Yad. Fiz.* **10** (1969) 409; H.D. Politzer, *Phys. Rev. Lett.* **30** (1973) 1346; S.Weinberg, *Phys. Rev. Lett.* **31** (1973) 494; *Phys. Rev.* **D8** (1973) 4482; D.J. Gross and F. Wilczek, *Phys. Rev. Lett.* **30** (1973) 1343; *Phys. Rev.* **D8** (1973) 3633. W. Kummer, *Acta Phys. Austriaca* **41** (1975) 315; N. Konetschny and W. Kummer, *Nucl. Phys.* **B100** (1975) 106; **B124** (1976) 145; J. Frenkel and J.C. Taylor, *Nucl. Phys.* **B109** (1976) 439.

17) N. Konetschny and W. Kummer, *Nucl. Phys.* **B108** (1976) 397; G.C. Rossi and M. Testa, *Nucl. Phys.* **B163** (1980) 109; N. Christ and T.D. Lee, *Phys. Rev.* **D22** (1980) 939.

Figure captions

Fig.1 : Box-isospin diagrams up to order g^6 for the two body interaction.

fig.2 : The set of three body eikonal diagrams under consideration.

fig.3 : Isospin diagram associated with the set of diagrams in fig.2.

Fig.4 : One of the graphs in fig.2 with the kinematical variables explicitly indicated.

Fig.5 : The three graphs corresponding to Eq.(1).

Fig.6 : Graphical representation of the commutation relations. The signs of the second addendum are the consequence of the convention for the ordering of the color indices in the triple gluon vertex (clockwise for +).

Fig.7 : The color factors G_i, $i = 1 \ldots 16$ in Eq.(12) and (14).

Fig.8 : The three different ways of cutting a graph that give a result different from zero.

Fig.9 : The graphs corresponding to Eq.(18).

Fig.10: The graphs corresponding to Eq.(25).

Fig.11: Graphs of kind "Two Box cuts, *case c*".

Fig.12: The graphs corresponding to Eq.(30).

Fig.13: The graphs corresponding to Eq.(34).

Fig.14: The graphs corresponding to Eq.(35) and Eq.(36).

Fig.15: Representation of the propagator in Eq.($A4$), 15 a), and eikonal diagram for the three body parton interaction, 15 b).

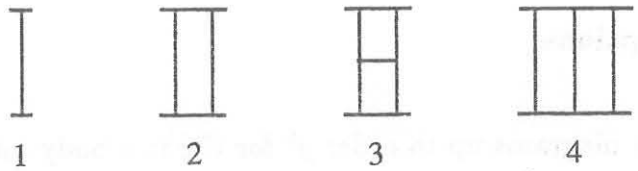

Fig. 1

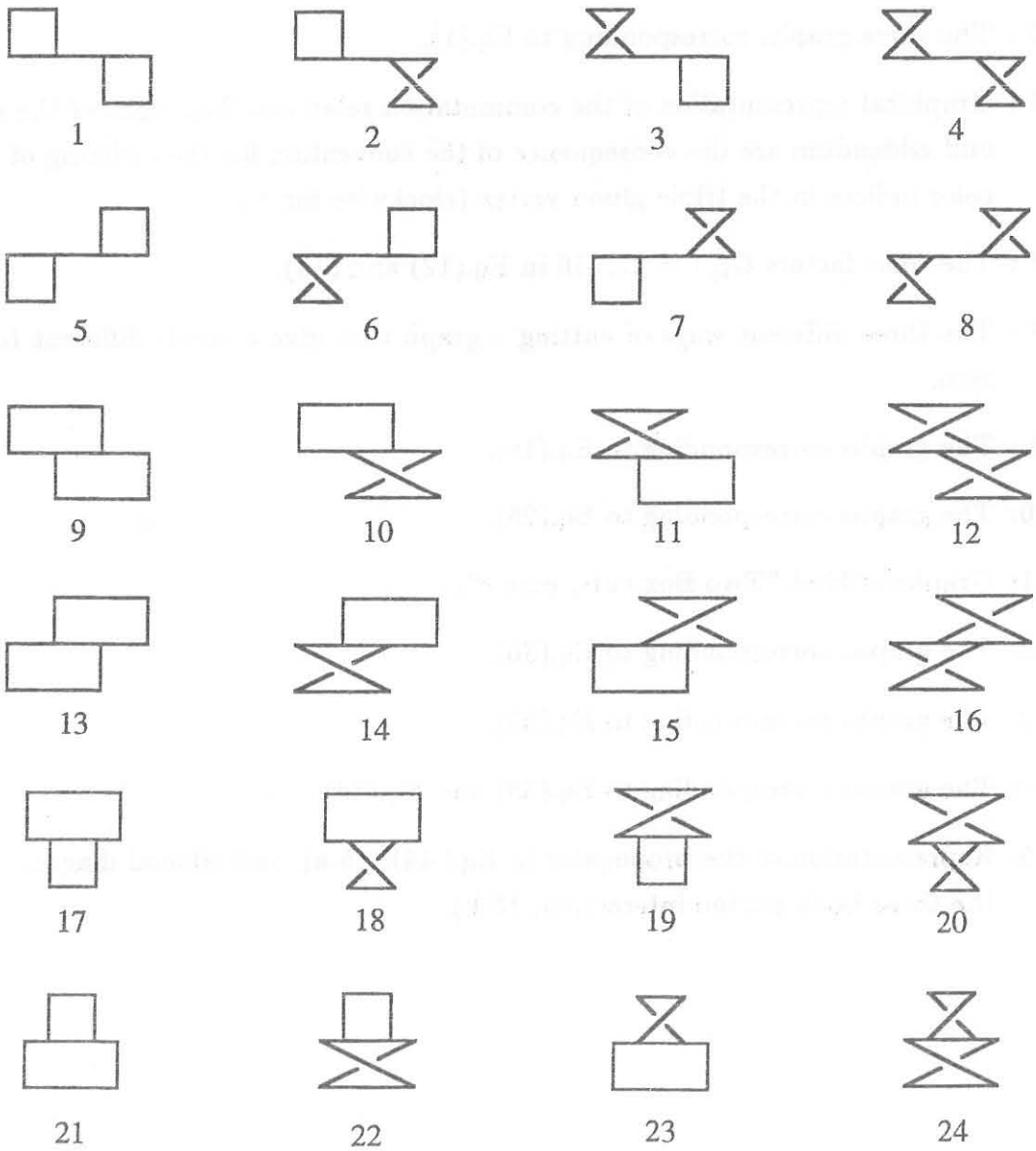

Fig. 2

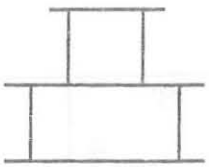

Fig. 3

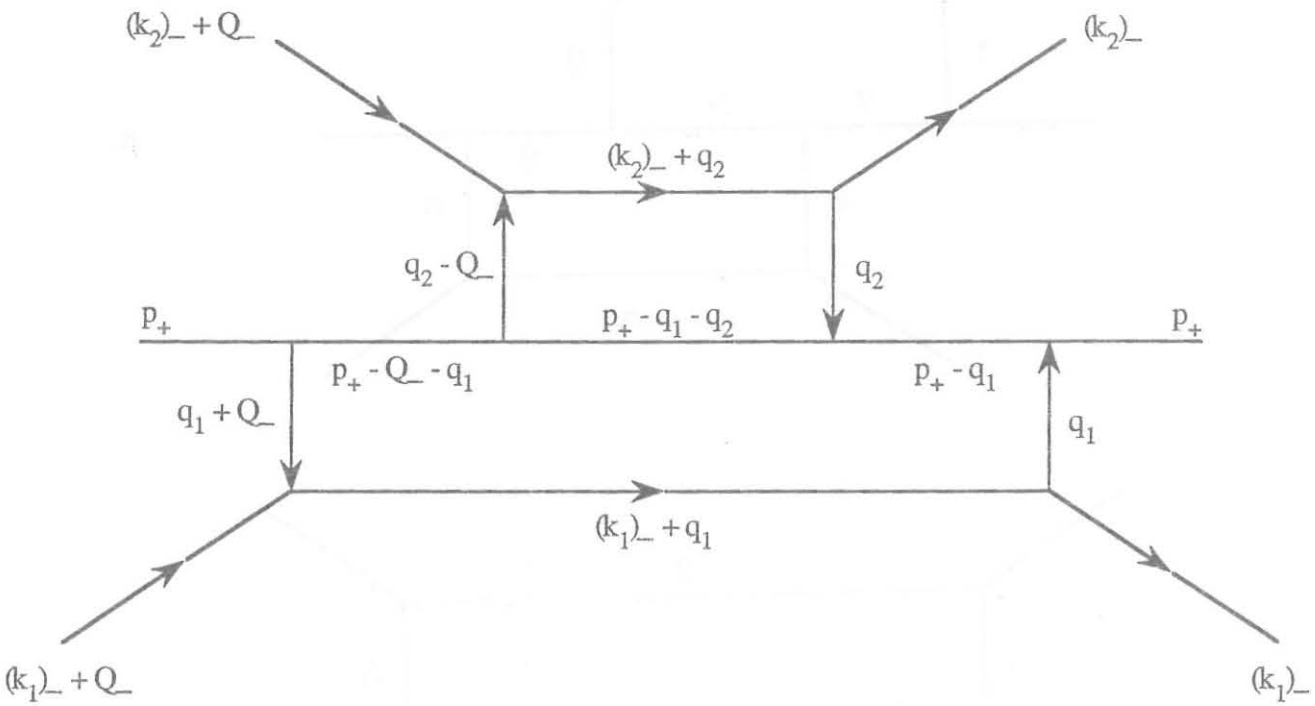

Fig. 4

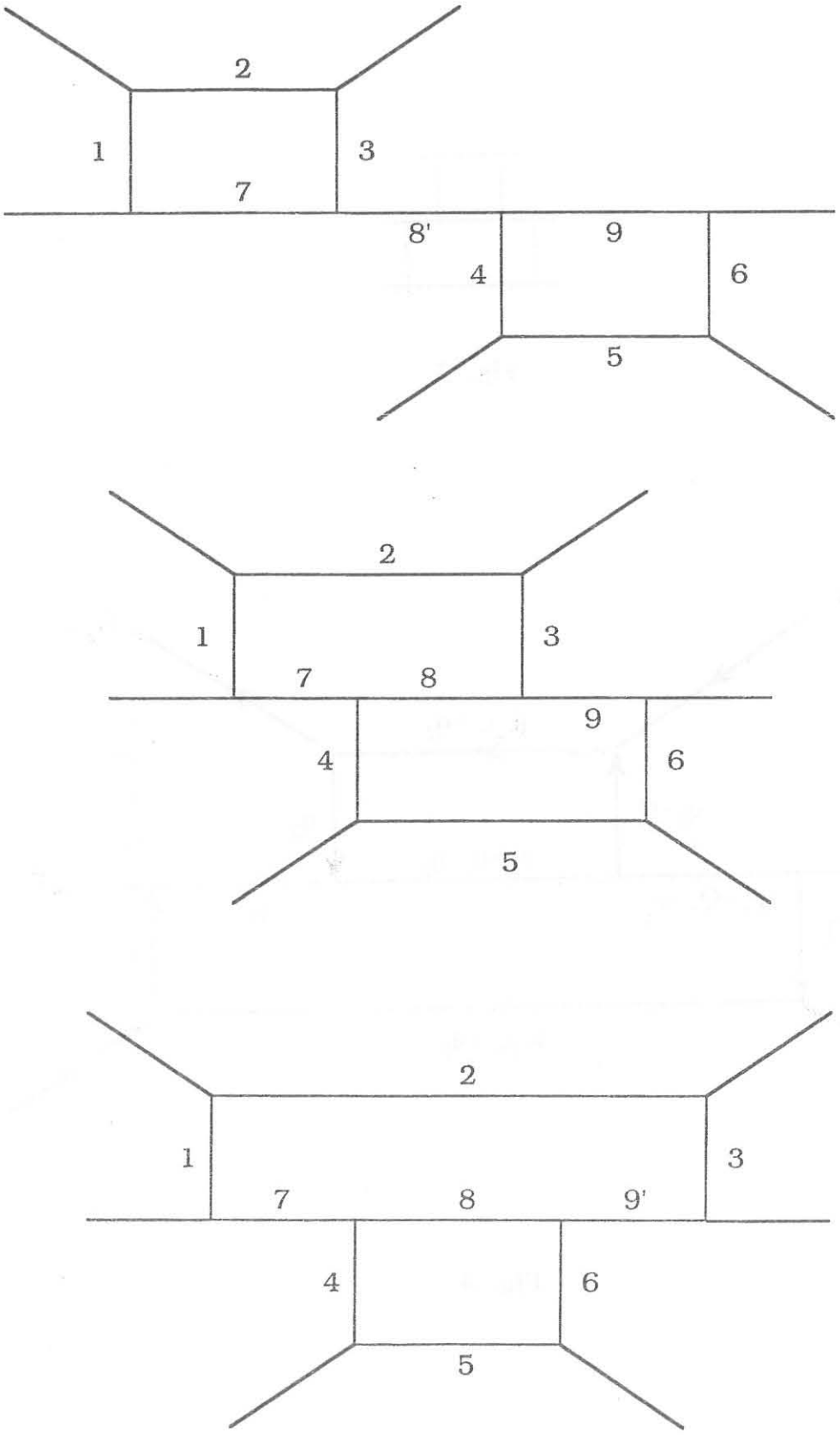

Fig. 5

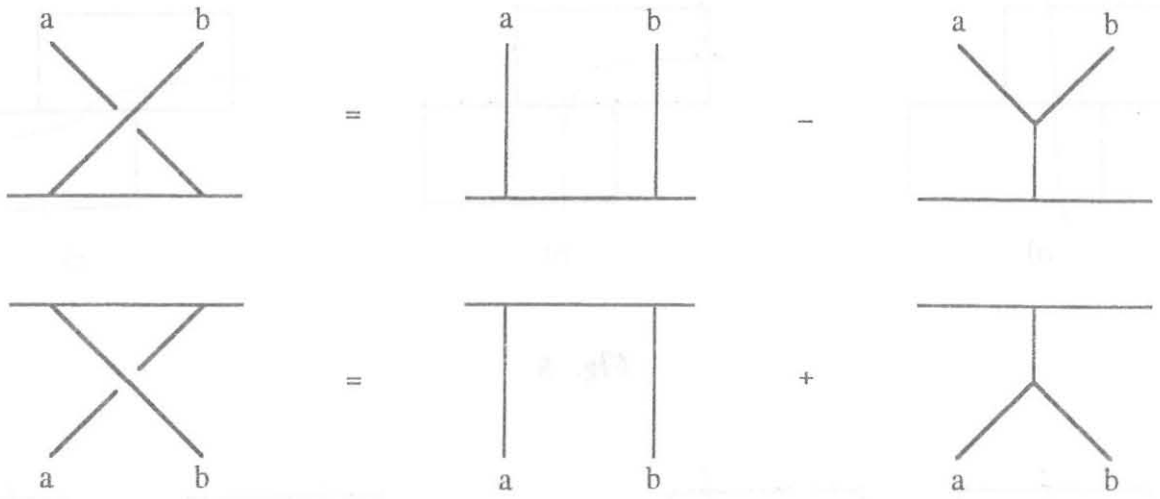

Fig. 6

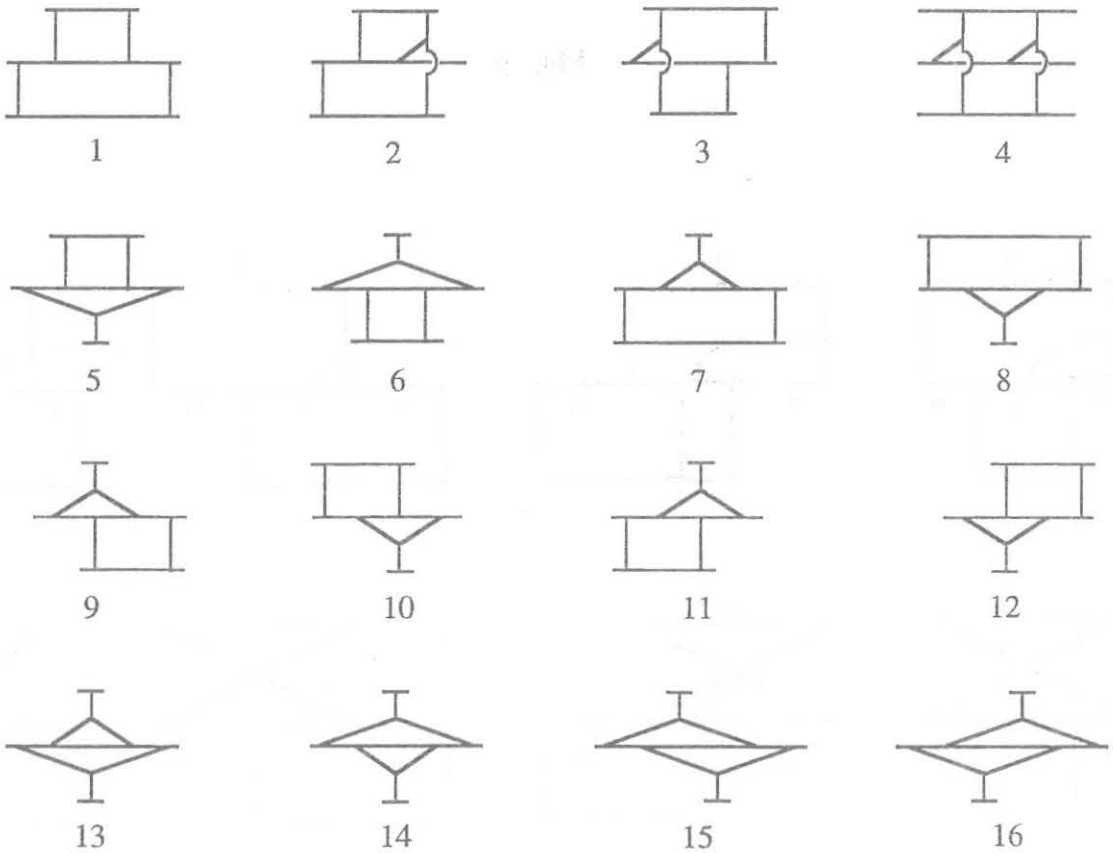

Fig. 7

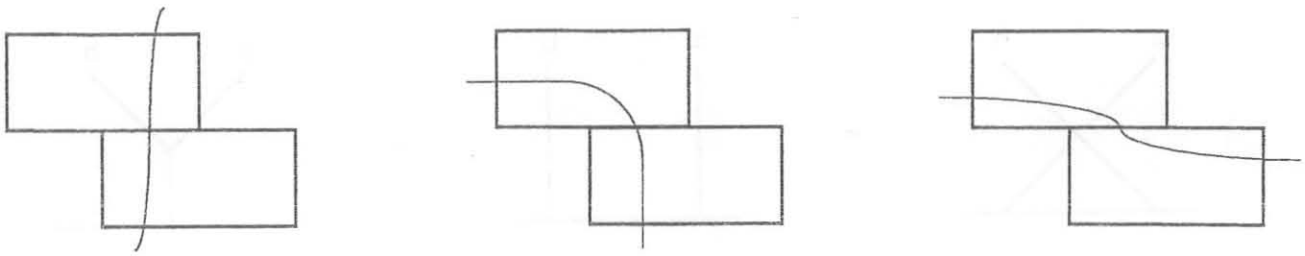

Fig. 8

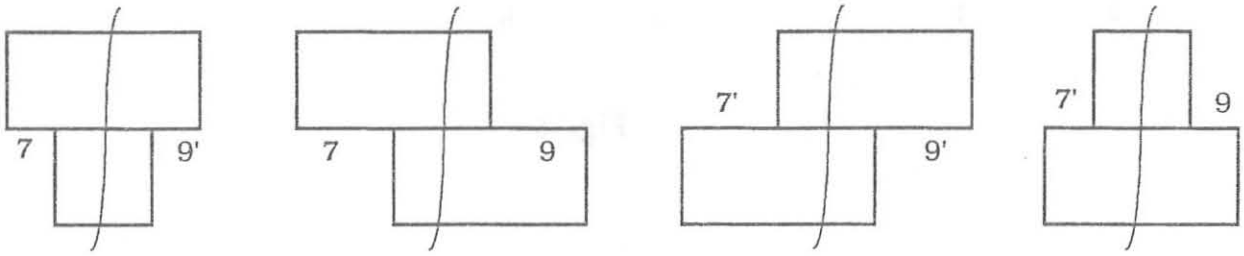

Fig. 9

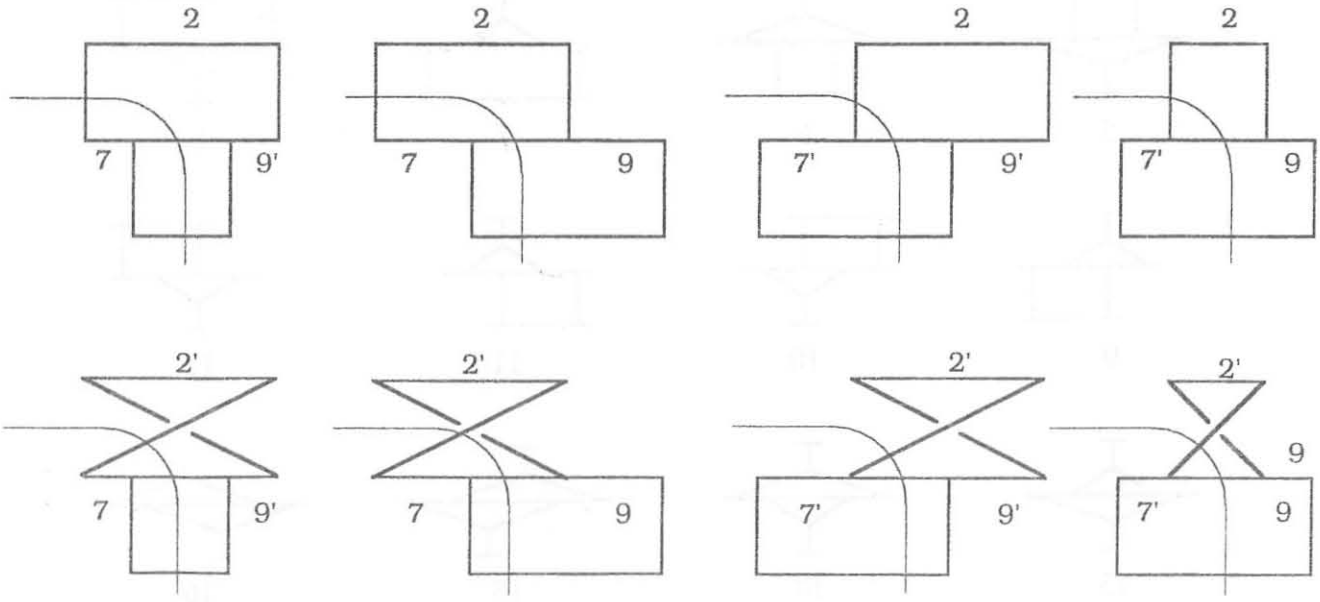

Fig. 10

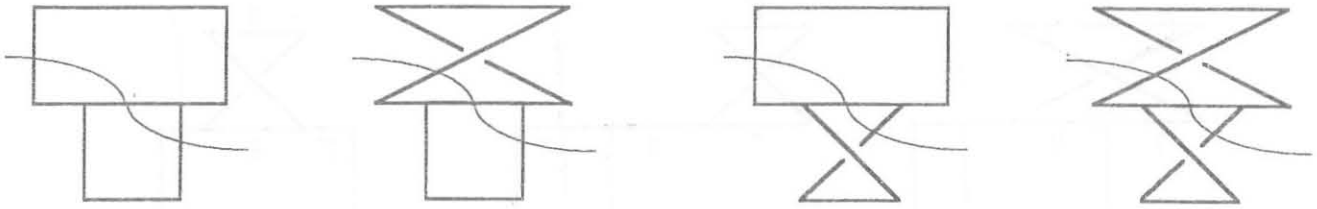

a)

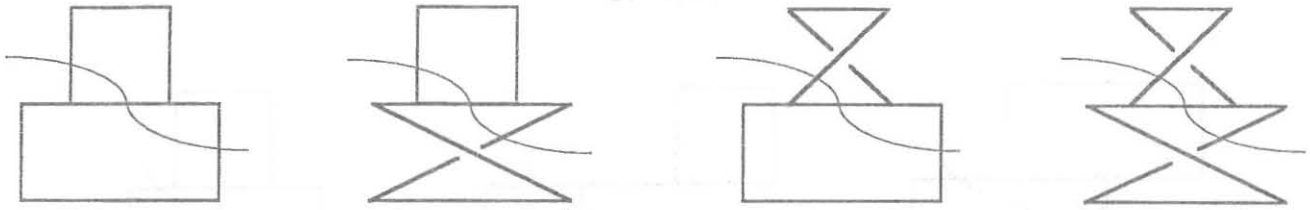

b)

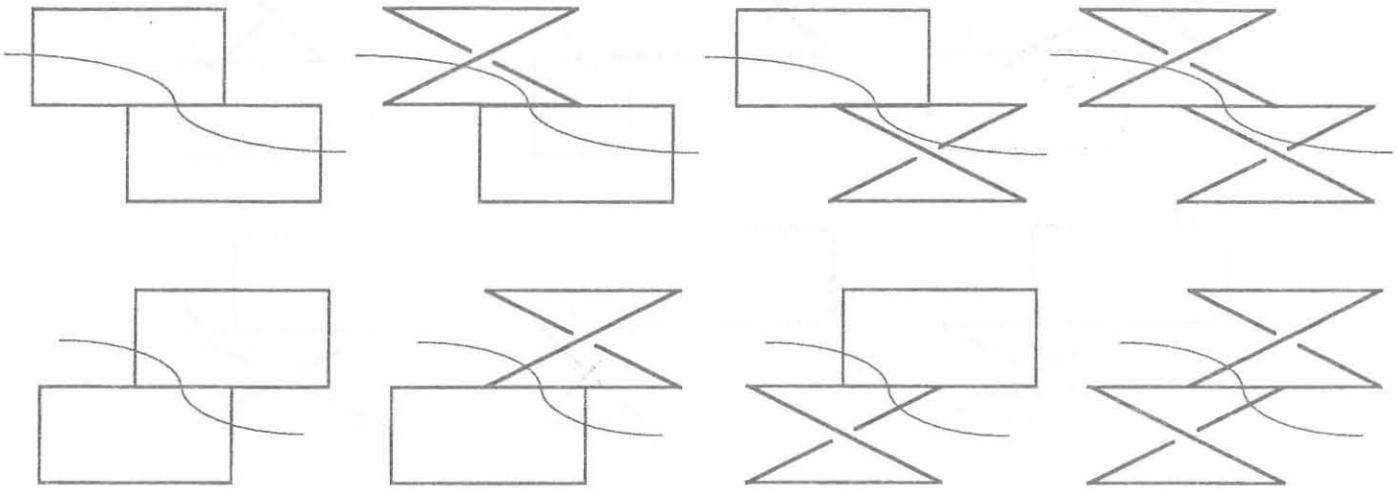

Fig. 11

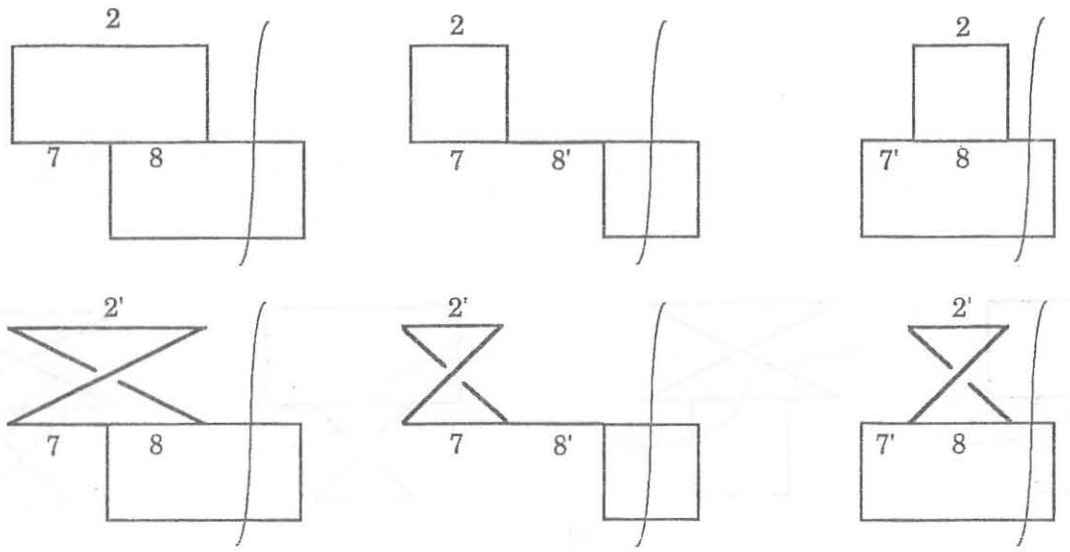

Fig. 12

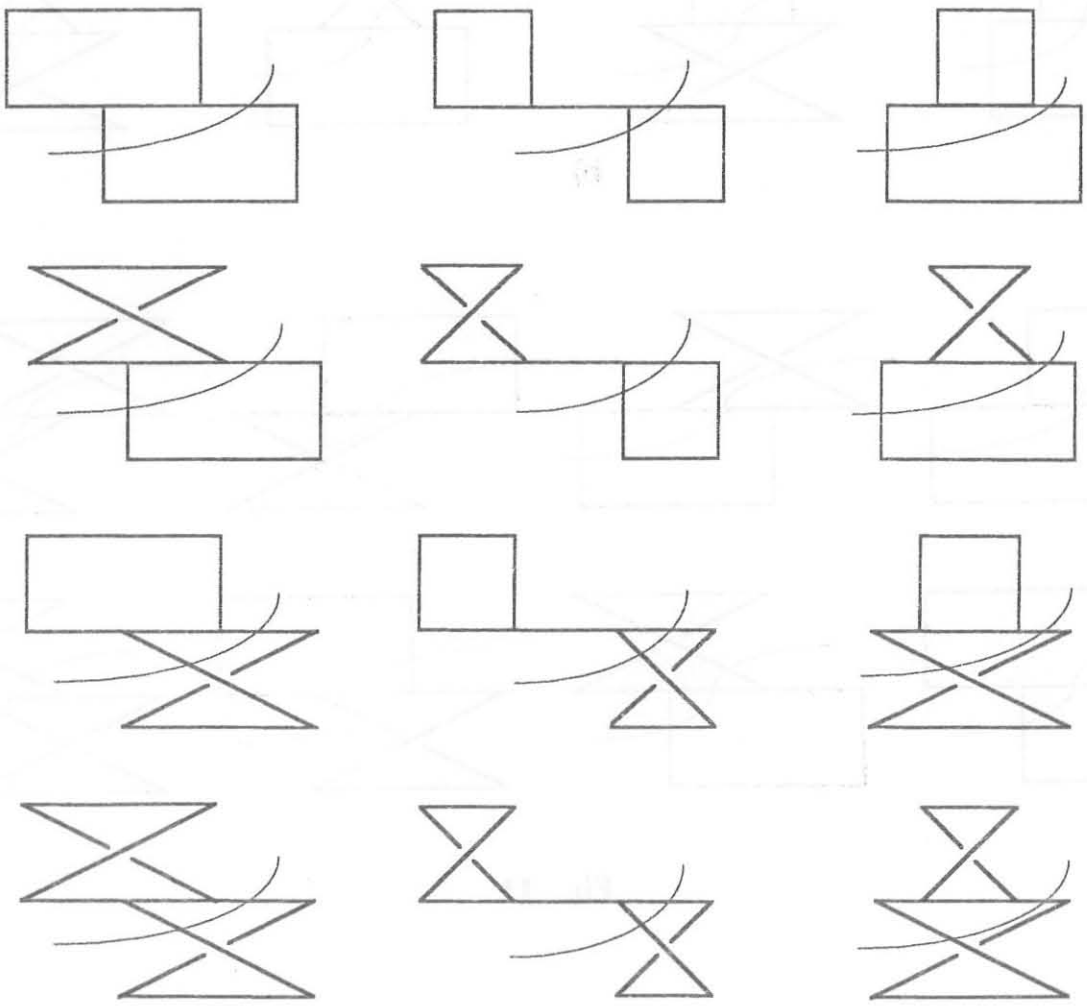

Fig. 13

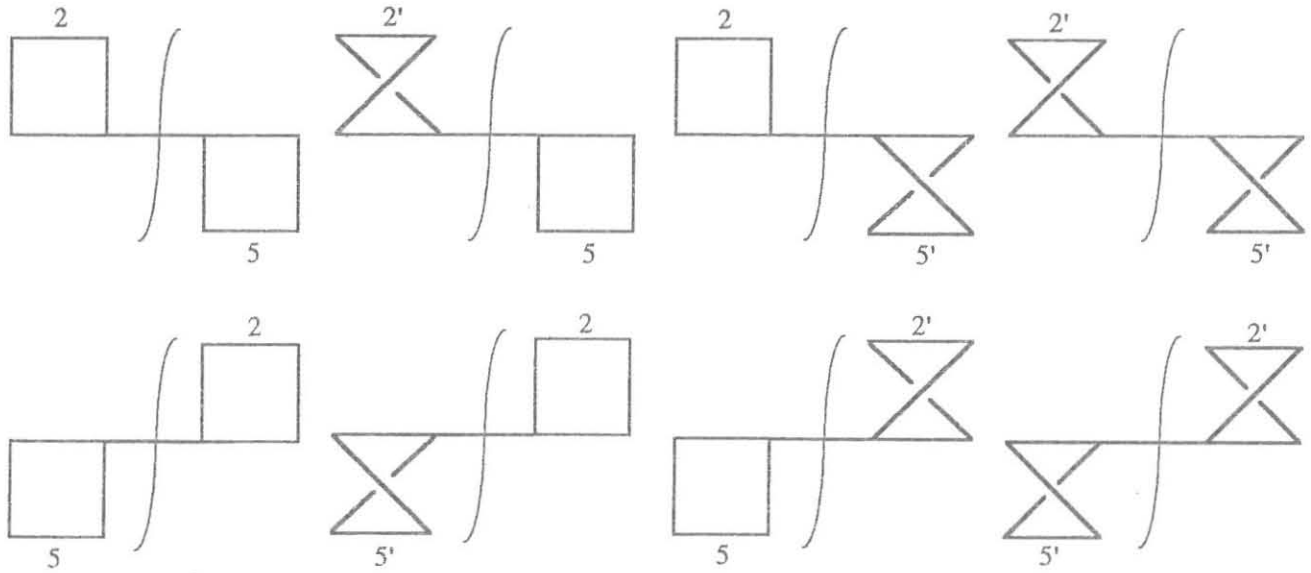

Fig. 14

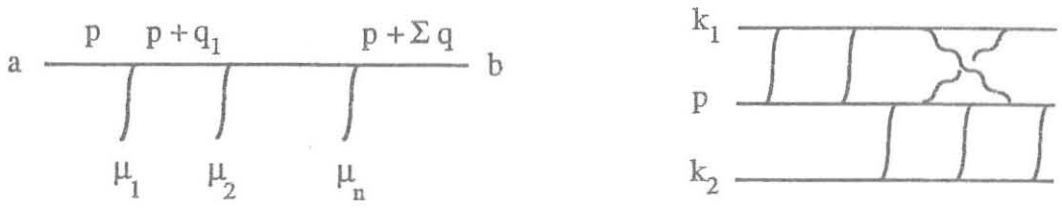

a) b)

Fig. 15